

Analysis of 26 Barium Stars \star, \star, \star

I. Abundances

D.M. Allen^{***} and B. Barbuy

Instituto de Astronomia, Geofísica e Ciências Atmosféricas, Universidade de São Paulo, Rua do Matão 1226, 05508-900 São Paulo, Brazil,
e-mail: dinah@astro.iag.usp.br, barbuy@astro.iag.usp.br

Received, 2006; accepted, 2006

ABSTRACT

Context. We present a detailed analysis of 26 barium stars, including dwarf barium stars, providing their atmospheric parameters (T_{eff} , $\log g$, $[\text{Fe}/\text{H}]$, v_t) and elemental abundances.

Aims. We aim at deriving gravities and luminosity classes of the sample stars, in particular to confirm the existence of dwarf barium stars. Accurate abundances of chemical elements were derived. Abundance ratios between nucleosynthetic processes, by using Eu and Ba as representatives of the r- and s-processes are presented.

Methods. High-resolution spectra with the FEROS spectrograph at the ESO-1.5m Telescope, and photometric data with Fotrap at the Zeiss telescope at the LNA were obtained. The atmospheric parameters were derived in an iterative way, with temperatures obtained from colour-temperature calibrations. The abundances were derived using spectrum synthesis for Li, Na, Al, α -, iron peak, s- and r-elements atomic lines, and C and N molecular lines.

Results. Atmospheric parameters in the range $4300 < T_{\text{eff}} < 6500$, $-1.2 < [\text{Fe}/\text{H}] < 0.0$ and $1.4 \leq \log g < 4.6$ were derived, confirming that our sample contains giants, subgiants and dwarfs. The abundance results obtained for Li, Al, Na, α - and iron peak elements for the sample stars show that they are compatible with the values found in the literature for normal disk stars in the same range of metallicities. Enhancements of C, N and heavy elements relative to Fe, that characterise barium stars, were derived and showed that $[\text{X}/\text{Ba}]$ vs. $[\text{Ba}/\text{H}]$ and $[\text{X}/\text{Ba}]$ vs. $[\text{Fe}/\text{H}]$ present different behaviour as compared to $[\text{X}/\text{Eu}]$ vs. $[\text{Eu}/\text{H}]$ and $[\text{X}/\text{Eu}]$ vs. $[\text{Fe}/\text{H}]$, reflecting the different nucleosynthetic sites for the s- and r-processes.

Key words. barium stars – atmospheric parameters – abundances

1. Introduction

Barium stars were recognized as a distinct group of peculiar stars by Bidelman & Keenan (1951). Initially, the objects included in this group were only G and K giants which showed strong lines of s-process elements, particularly Ba II at $\lambda 4554 \text{ \AA}$ and Sr II at $\lambda 4077 \text{ \AA}$, as well as enhanced CH, CN and C_2 molecular bands. However, the discovery by Tomkin et al. (1989) that the dwarf star HR 107 showed chemical composition similar to that of a mild barium giant, has pushed the

search for less evolved barium stars (Gómez et al. 1997). Some studies have proposed that these stars could be ancestors of the barium giants (North et al. 1994; Barbuy et al. 1992).

McClure et al. (1980) revealed that most barium stars, maybe all of them, show variations in radial-velocity suggesting the presence of companions. This has been confirmed by McClure (1983, 1984) and Udry et al. (1998a,b). Böhm-Vitense (1980) and Böhm-Vitense & Johnson (1985) observed an ultraviolet excess in the barium stars ζ CAP and ξ Ceti, which could be explained by white dwarf companions.

The binarity hypothesis for all barium stars has provided an interesting explanation for their peculiarity. In this context, the more massive of them evolves through the thermal pulse - asymptotic giant branch (TP-AGB) phase, when s-process occurs, and afterwards the third dredge-up brings to the surface carbon and s-process elements. The enriched material is then transferred to the companion, which becomes a barium star. Bond et al. (2003) observed a planetary nebula (PN) in Cassiopeia, with a late type star, showing overabundance in

Send offprint requests to: D.M. Allen

* Based on spectroscopic observations collected at the European Southern Observatory (ESO), within the Observatório Nacional ON/ESO and ON/IAG agreements, under FAPESP project n° 1998/10138-8. Photometric observations collected at the Observatório do Pico dos Dias (LNA/MCT).

** Tables 5 and 15 are only available in electronic at the CDS via anonymous ftp to cdsarc.u-strasbg.fr/Abstract.html

*** Present address: Observatório do Valongo/UFRJ, Ladeira do Pedro Antonio 43, 20080-090 Rio de Janeiro, RJ, Brazil

carbon and s-process elements typical of a barium star. This discovery confirmed the hypothesis about their origin. In the PNs Abell 35 (Jacoby 1981; Thévenin & Jasniewicz 1997) and LoTr5 (Jasniewicz et al. 1996; Thévenin & Jasniewicz 1997) barium and s-elements rich stars were also observed. There is a central hot star in each of these nebulae detected with IUE (*International Ultraviolet Explorer*). Jeffries & Smalley (1996) observed the binary system 2REJ0357+283 consisting of a white dwarf and an s-element rich K dwarf star, where the high rotation can be attributed to the mass transfer from the white dwarf progenitor, during the AGB phase.

However, several IUE spectra of barium stars analysed by Dominy & Lambert (1983) showed no UV excess, putting in check the hypothesis that all barium stars have a white dwarf companion. Böhm-Vitense et al. (2000) observed UV excess for most of their barium stars, but the estimated cooling time for some of the companion white dwarfs, was too long or larger than the evolution time of the barium star. If the binarity hypothesis is not confirmed for all stars of the group, another explanation for their origin would be needed.

In Sect. 2 the observations are reported. In Sect. 3 the atmospheric parameters are derived. In Sect.4 the abundances derivation is described. In Sect. 5 conclusions are drawn.

2. Observations

The sample stars were selected from Gómez et al. (1997) and North et al. (1994) where the authors suggested that there were less evolved barium stars among the giants of their sample. The star HR 107 from Tomkin et al. (1989) was also included in the sample. Mennessier et al. (1997) identified HD 5424, HD 13551, HD 116869 and HD 123396 as halo stars.

Optical spectra were obtained at the 1.52m telescope at ESO, La Silla, using the Fiber Fed Extended Range Optical Spectrograph (FEROS) (Kaufer et al. 2000), on February and October/2000, January and October/2001, January and July/2002. The total spectrum coverage is 356-920 nm with a resolving power of 48,000. Two fibers, with entrance aperture of 2.7 arcsec, recorded simultaneously star light and sky background. The detector is a back-illuminated CCD with 2948×4096 pixels of 15 μ m size. Reductions were carried out through a special pipeline package for reductions (DRS) of FEROS data, in MIDAS environment. The data reduction proceeded with subtraction of bias and scattered light in the CCD, orders extraction, flatfielding, and wavelength calibration with a ThAr calibration frame. Radial velocities were taken into account by using IRAF tasks RVIDLINE and DOPCOR. The spectra were cut in parts of 100 Å each using the SCOPY task, and the normalization was carried out with the CONTINUUM task.

The photometric observations were obtained using the FOTRAP (Fotômetro Rápido) at the ZEISS 60cm telescope at LNA (Laboratório Nacional de Astrofísica) in June, August and September/2001 and May and July/2002. Data reductions were done using the appropriate code available at LNA. The colours obtained were (B-V), (V-R), (R-I) and (V-I). The log of observations is presented in Table 1.

Table 1. Log of spectroscopic (*sp*) and photometric (*pho*) observations. The S/N ratio was measured in the of λ 5000 Å region. Radial velocity v_r (km/s) is shown in column 6. References used to build this sample: 1 - Gómez et al. (1997); 2 - North et al. (1994); 3 - Tomkin et al. (1989).

star	date _{pho}	date _{sp}	Exp. (s)	S/N	v_r	ref
HD749	31/08/2001	17/01/2001	1800	200	15.47	1
HR107	16/07/2002	05/10/2001	600	200	9.76	3
HD5424	01/09/2001	17/01/2001	3000	100	-1.56	1
HD8270	01/09/2001	14/02/2000	1800	150	14.97	1
HD12392	31/08/2001	17/01/2001	2700	120	-25.38	1
HD13551	01/09/2001	14/02/2000	2700	100	34.79	1
HD22589	01/09/2001	14/02/2000	2700	200	-28.90	1
HD27271	01/09/2001	14/02/2000	1800	250	-16.65	1
HD48565	...	23/01/2002	600	250	-33.67	2
HD76225	18/05/2002	23/01/2002	1200	150	-1.34	2
HD87080	18/05/2002	14/02/2000	2700	120	8.10	1
HD89948	18/05/2002	14/02/2000	1800	250	6.01	1
HD92545	18/05/2002	23/01/2002	1200	150	-0.16	2
HD106191	19/05/2002	03/07/2002	3600	100	0.68	2
HD107574	18/05/2002	23/01/2002	1320	200	0.78	2
HD116869	18/05/2002	14/02/2000	3600	150	-9.84	1
HD123396	19/05/2002	15/02/2000	3600	150	26.64	1
HD123585	18/05/2002	04/07/2002	7200	100	27.87	1,2
HD147609	18/05/2002	04/07/2002	3600	120	-19.39	2
HD150862	18/05/2002	04/07/2002	3600	150	50.38	2
HD188985	19/05/2002	04/10/2001	1800	130	8.17	1,2
HD210709	26/06/2001	18/10/2000	2700	100	27.01	1
HD210910	27/06/2001	19/10/2000	2400	200	-9.86	1
HD222349	15/07/2002	02/10/2001	2400	150	27.65	2
BD+185215	...	05/10/2001	3600	100	-33.98	2
HD223938	15/07/2002	18/10/2000	2700	250	-0.85	1

3. Atmospheric Parameters

3.1. Extinction

Reddening values shown in Table 3 were derived according to Cardelli et al. (1989), using effective wavelengths by Bessell & Brett (1988) and Bessell (1979). The visual extinction A_v was considered null for stars nearer than 70 pc according to Vergely et al. (1998), and for the other stars, A_v was determined according to Chen et al. (1998).

Distances were taken from Mennessier et al. (1997). Including Hipparcos parallaxes as input, these authors used a Maximum Likelihood method, which they considered to provide better results for the distances than the ones obtained directly from the parallaxes. The distances missing in Mennessier et al., were obtained directly from Hipparcos parallaxes. In cases where no parallax values were available in the Hipparcos Catalogue, initial distances were estimated assuming that these stars are subgiants of absolute magnitude $M_v = 3.3$ from Gómez et al. (1997), or dwarfs of $M_v = 4.5$. The V magnitudes in these cases were taken from SIMBAD available at the web address <http://simbad.u-strasbg.fr/Simbad>. Distances are shown in Table 2.

Table 2. Equatorial and galactic coordinates of the sample barium stars. The errors on last decimals are given in parenthesis. Distances D_M are from Mennessier et al. (1997); distances D_H were determined from Hipparcos parallaxes ($D_H=1/\pi_H$); D_g are the distances from spectroscopy for stars with Hipparcos parallax not available.

star	α (2000)	δ (2000)	π_H (mas)	D_H (kpc)	D_M (kpc)	D_g (kpc)	l	b
HD 749	00:11:38	-49:39:20	7.11(1.08)	0.141(20)	0.161(23)	...	319.03	-66.21
HR 107	00:28:20	+10:11:23	27.51(0.86)	0.036(1)	113.62	-52.26
HD 5424	00:55:44	-27:53:36	0.22(1.42)	4.5(20.0)	0.979(344)	...	251.97	-88.78
HD 8270	01:21:10	-47:31:48	13.43(1.16)	0.074(6)	0.078(7)	...	288.97	-68.78
HD 12392	02:01:23	-04:48:10	0.219(30)	162.77	-62.14
HD 13551	02:10:09	-60:45:31	8.91(0.88)	0.112(10)	0.118(12)	...	286.75	-53.83
HD 22589	03:37:55	-06:58:25	0.249(20)	193.68	-45.71
HD 27271	04:18:34	+02:28:17	6.01(1.13)	0.166(30)	0.168(15)	...	190.74	-32.02
HD 48565	06:44:55	+20:51:38	21.77(1.07)	0.046(2)	0.046(2)	...	193.53	+7.97
HD 76225	08:54:01	-26:54:56	3.37(1.11)	0.297(98)	0.208(32)	...	251.43	+11.42
HD 87080	10:02:01	-33:41:11	7.90(1.39)	0.127(22)	0.160(27)	...	267.02	+17.12
HD 89948	10:22:22	-29:33:23	23.42(0.93)	0.043(2)	0.043(2)	...	268.02	+23.03
HD 92545	10:40:58	-12:11:44	7.82(1.05)	0.128(17)	0.120(13)	...	259.85	+39.52
HD 106191	12:13:11	-15:13:56	0.145(20)	289.43	+46.63
HD 107574	12:21:52	-18:24:00	5.02(1.06)	0.199(42)	293.17	+43.91
HD 116869	13:26:38	-04:26:46	0.23(1.34)	4.3(25.3)	0.703(172)	...	319.33	+57.30
HD 123396	14:17:33	-83:32:52	1.73(0.86)	0.578(287)	0.834(295)	...	305.46	-21.10
HD 123585	14:09:36	-44:22:01	8.75(1.39)	0.114(18)	0.121(11)	...	317.36	+16.30
HD 147609	16:21:52	+27:22:27	16.64(0.99)	0.060(4)	45.97	+43.60
HD 150862	16:44:44	-25:12:59	0.74(10)	355.20	+13.21
HD 188985	19:59:58	-48:58:32	14.06(1.18)	0.071(6)	0.074(6)	...	350.01	-31.07
HD 210709	22:12:54	-35:25:51	-0.10(1.37)	...	0.197(29)	...	9.08	-55.37
HD 210910	22:13:42	-03:46:31	6.13(1.16)	0.163(31)	0.195(32)	...	57.73	-45.72
HD 222349	23:40:01	-56:44:26	0.168(20)	321.31	-57.77
BD+18 5215	23:46:56	+19:28:22	0.153(20)	102.68	-40.85
HD 223938	23:53:50	-50:00:00	4.42(1.21)	0.226(62)	0.218(36)	...	324.82	-64.61

Table 3. Reddening values for sample stars (see Sect. 3.1).

star	A_V	E(B-V)	E(V-I)	E(V-R)	E(R-I)	E(V-K)
HD 749	0.0(1)
HR 107	0.0(1)
HD 5424	0.0(1)
HD 8270	0.0(1)
HD 12392	0.0(1)
HD 13551	0.0(1)
HD 22589	0.030(108)	0.010	0.012	0.005	0.007	0.027
HD 27271	0.092(123)	0.029	0.036	0.015	0.021	0.082
HD 48565	0.0(1)
HD 76225	0.038(109)	0.012	0.015	0.006	0.009	0.034
HD 87080	0.161(140)	0.052	0.063	0.027	0.037	0.143
HD 89948	0.0(1)
HD 92545	0.045(111)	0.014	0.018	0.007	0.010	0.040
HD 106191	0.018(105)	0.006	0.007	0.003	0.005	0.016
HD 107574	0.037(109)	0.012	0.015	0.006	0.009	0.033
HD 116869	0.0(1)
HD 123396	0.061(115)	0.020	0.024	0.010	0.014	0.054
HD 123585	0.130(132)	0.042	0.051	0.022	0.030	0.115
HD 147609	0.0(1)
HD 150862	0.090(123)	0.029	0.035	0.015	0.021	0.080
HD 188985	0.051(113)	0.016	0.020	0.008	0.012	0.045
HD 210709	0.0(1)
HD 210910	0.026(106)	0.008	0.010	0.004	0.006	0.023
HD 222349	0.0(1)
BD+18 5215	0.047(112)	0.015	0.019	0.008	0.011	0.042
HD 223938	0.0(1)

3.2. Temperatures

Literature photometric data were taken from the 2MASS Point Source Catalog (Cutri et al. 2003, K_s magnitude), The

General Catalogue Photometric Data by J.C. Mermilliod, B. Hauck and M. Mermilliod available at the web address <http://obswww.unige.ch/gcpd/gcpd.html> (B_1 , B_2 , G and V_1 magnitudes from Geneva system), Hipparcos Catalogue (Perryman et al. 1997, $(B-V)_H$ and V, shown in the columns 3 and 8 of Table 4, respectively). For sample stars missing in the Hipparcos Catalogue, $(B-V)$ values were taken from SIMBAD. Photometric data used are shown in Table 4.

The colour-temperature calibrations were adopted from Alonso et al. (1996) for stars of $\log g > 3.6$, Alonso et al. (1999) for $\log g \leq 3.6$ and Lejeune et al. (1998) for all stars. Alonso et al. calibrations use the Johnson system for UBVR and TCS (Telescopio Carlos Sánchez) for JHKLHMN. Lejeune et al. used the Cousins system for UBVR and MSO for JHKLHMN. The calibrations used for the Geneva colours were adopted from Meléndez & Ramirez (2003) for dwarfs and Ramírez & Meléndez (2004) for giants. The transformations between photometric systems were obtained from Carpenter (2001), Bessell & Brett (1988), Alonso et al. (1996) and Alonso et al. (1999).

The G band affects the spectrum in the $\lambda < 4320\text{\AA}$ region. It is possible to see some alteration in the black body distribution in the far infrared, probably due to dust in the binary system (Catchpole et al. 1977; Hakkila 1989). The colour $(B-V)$ is affected by the CN and C_2 bands, causing in the spectrum the depression of Bond & Neff (1969), making the stars red-

der and as a consequence the temperatures derived from this colour can be lower. Colours (R-I) and (V-I) are more affected by molecular bands and blanketing effects in K and M stars than (V-K). The calibrations resulted in slightly different temperatures. In general, Lejeune et al. (1998) provide higher temperatures than Alonso et al. (1996) and Alonso et al. (1999). The resulting temperatures of the Geneva system are generally higher than those from the (B-V) index (see Tables 6 and 7). Given that some indicators tend to increase and others to reduce the temperature, effective temperatures adopted were the mean values obtained from the (B-V) Hipparcos, (B-V), (V-I), (V-R) and (R-I) from LNA, and (V-K) 2MASS indices and the colours of the Geneva system (B_2-V_1), (B_2-G) and (B_1-B_2). This is shown in column 2 of Table 9. The uncertainties were estimated to be ± 100 K, taking into account the errors from the colour-temperature calibrations.

In order to check photometric temperatures, the excitation temperatures T_{exc} were derived by imposing excitation equilibrium. Lines of Fe I and Fe II that give metallicities differing between the average and median of $\Delta[\text{Fe}/\text{H}] > 0.01$ dex were eliminated. This procedure prevents blended lines to affect the results. Resulting T_{exc} are given in column 3 of Table 9, and illustrated in Figure 1.

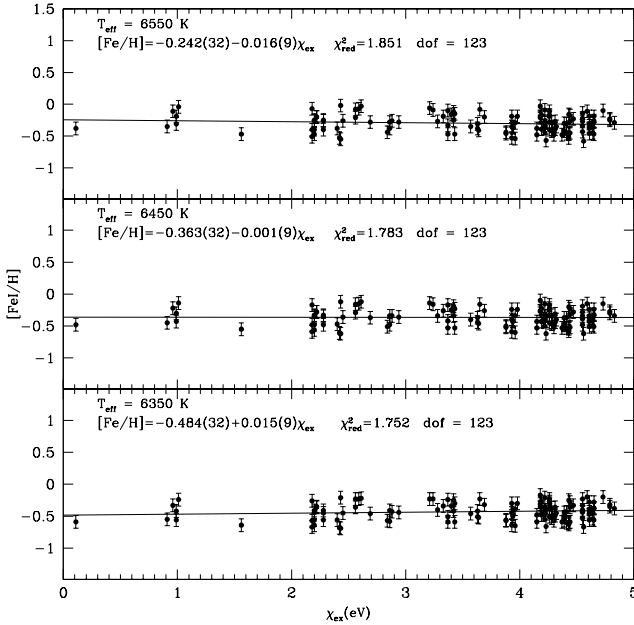


Fig. 1. $[\text{Fe}/\text{H}]$ vs. χ_{ex} (eV) for the star HD 123585. Least-squares fits for 3 values of temperatures were used to derive T_{exc} . Uncertainties on $[\text{Fe}/\text{H}]$ and χ_{ex} were estimated to be ± 0.10 and ± 0.01 , respectively.

3.3. Surface Gravity

Surface gravities ($\log g$) were determined using two methods:

1) Spectroscopic gravities were derived by imposing ionization equilibrium of Fe I and Fe II (Figure 3), and given in

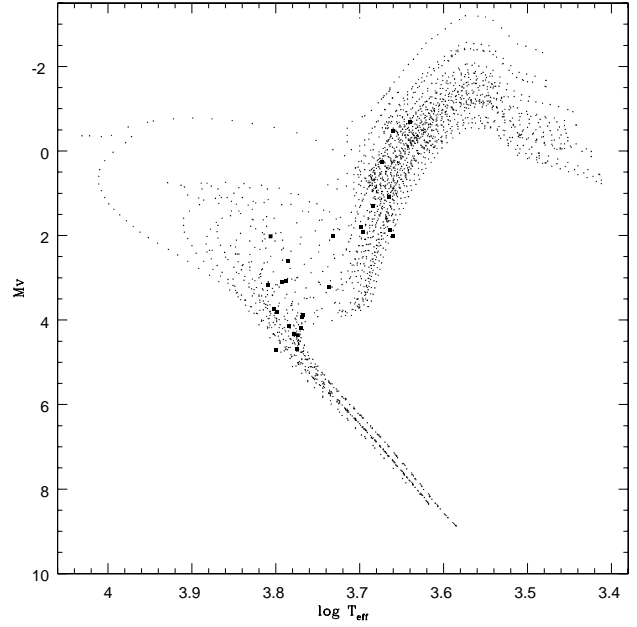


Fig. 2. Isochrones from Bertelli et al. (1994) with sample stars overlotted (black squares).

column 4 of Table 9. The gravity $\log g$ was varied until the two curves of growth give a same $[\text{Fe}/\text{H}]$ value, where Fe II lines are more sensitive to gravity variations. According to Nissen et al. (1997), this method presents a problem because Fe I lines are affected by NLTE effects. The uncertainty was estimated as ± 0.1 dex.

2) The classical equations of stellar evolution (equation 1) as a function of the distances, according to Nissen et al. (1997) and Allende Prieto et al. (1999):

$$\log\left(\frac{g_*}{g_\odot}\right) = \log\left(\frac{M_*}{M_\odot}\right) + 4 \log\left(\frac{T_{eff*}}{T_{eff\odot}}\right) + 0.4V_o + 0.4BC + 2 \log \frac{1}{D} + 0.1 \quad (1)$$

$$\sigma_{\log g} = \left[\left(\frac{\sigma_M}{M \ln(10)} \right)^2 + \left(\frac{4\sigma_{T_{eff*}}}{T_{eff*} \ln(10)} \right)^2 + \left(\frac{4\sigma_{T_{eff\odot}}}{T_{eff\odot} \ln(10)} \right)^2 + \sigma_{\log g_\odot}^2 + (0.4\sigma_{V_o})^2 + (0.4\sigma_{BC})^2 + \left(\frac{2\sigma_\pi}{\pi \ln(10)} \right)^2 \right]^{0.5} \quad (2)$$

where M_* is the stellar mass, V_o is the V corrected magnitude, BC is the bolometric correction and D is the distance derived as explained in Sect. 3.1. For the Sun, $T_{eff\odot} = 5781$ K (Bessell et al. 1998); $\log g_\odot = 4.44$; $M_{bol\odot} = 4.75$ (Cram 1999) were adopted.

Stellar masses in equation 1 were adopted from Bertelli et al. (1994) isochrones, as shown in Figure 2, and reported in column 9 of Table 10, corresponding to metallicities and temperatures as close as possible to those of the sample (columns 7 (or 6) and 2 of Table 9, respectively).

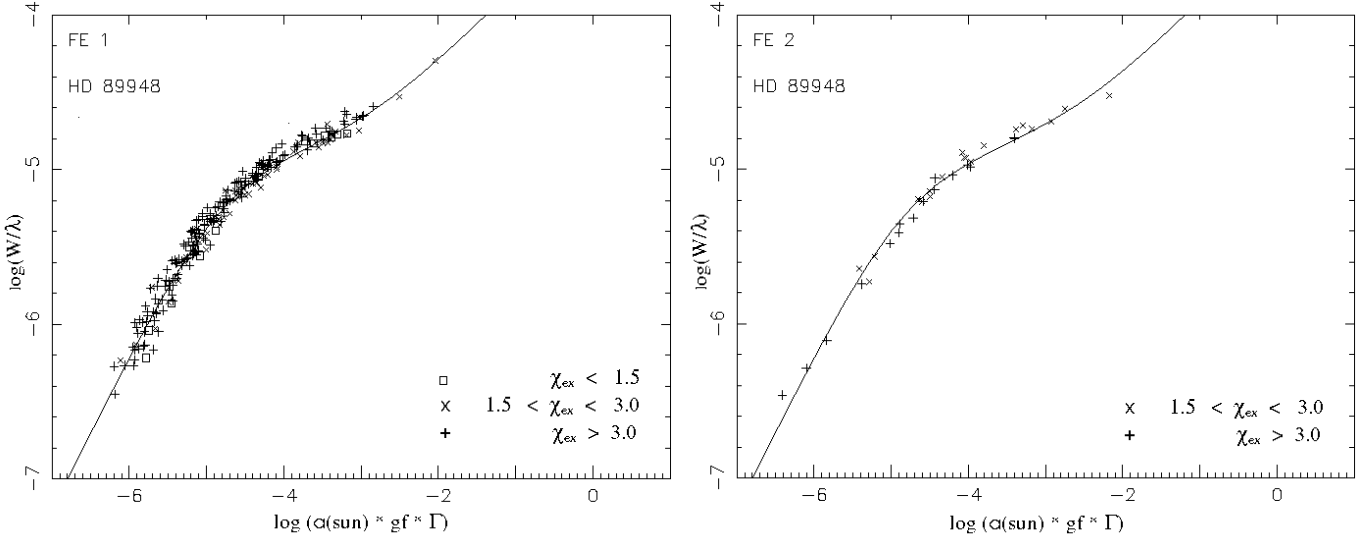


Fig. 3. Fe I and Fe II curves of growth for the star HD 89948. 'W' are the equivalent widths. $\log(\alpha(\text{sun})) = \log(n_x/n_H)$, where n_x and n_H are the numerical densities of an element and hydrogen, respectively; $\log gf$: oscillator strength; $\Gamma = (W/\lambda)(n_H/n_x)(gf)^{-1}$, as defined in Cayrel & Jugaku (1963) and Spite & Spite (1975). The iron abundance is given by the horizontal distance between the linear part of the curve of growth and the 45° line through the origin.

Uncertainties were estimated as $\pm 0.1 M_\odot$. These $\log g$ values are shown in column 5 of Table 9.

According to Nissen et al. (1997), the gravities resulting from the first method are systematically lower than those of the second, but there is no clear explanation. It could reside in NLTE effects in Fe I lines, uncertainties on masses or temperatures.

3.4. Oscillator Strengths

The Fe I line list and respective oscillator strengths from National Institute of Standards & Technology (NIST) library (Martin et al. 1988, 2002) and Fe II oscillator strengths renormalized by Meléndez & Barbuy (2006) were adopted. The list of Fe I and Fe II lines is given in Table 5. Damping constants for neutral lines were computed using the collisional broadening theory of Barklem et al. (1998, 2000, and references therein), as described in Zoccali et al. (2004) and Coelho et al. (2005). The oscillator strengths for the elements other than Fe and respective sources are shown in Table 15. For α - and iron peak elements, most values are from NIST. Laboratory values were preferred over theoretical ones.

For lines of Cu I, Eu II, La II, Ba II and Pb I, hyperfine structure (hfs) was taken into account employing a code made available by McWilliam, following the calculations described by Prochaska et al. (2000). The hfs constants were taken from Rutten (1978) for Ba II, Lawler et al. (2001a) for La II, Lawler et al. (2001b) for Eu II and Biémont et al. (2000) for Pb I. The final hfs components were determined by using the solar isotopic mix by Lodders (2003) and total $\log gf$ values from laboratory measurements, as shown in Table 15. For copper, the hfs from Biehl (1976) was used, with isotopic fractions of 0.69 for ^{63}Cu and 0.31 for ^{65}Cu . In this case, small corrections were applied such that the total $\log gf$ equals the gf -value

adopted in this work. The lines for which hfs were used were checked using the solar spectrum (Kurucz et al. 1984).

Table 5. Equivalent widths and atomic constants for Fe I and Fe II lines. e1 - HD 749; e2 - HR 107; e3 - HD 5424; e4 - HD 8270; e5 - HD 12392; e6 - HD 13551; e7 - HD 22589; e8 - HD 27271; e9 - HD 48565; e10 - HD 76225; e11 - HD 87080; e12 - HD 89948; e13 - HD 92545; e14 - HD 106191; e15 - HD 107574; e16 - HD 116869; e17 - HD 123396; e18 - HD 123585; e19 - HD 147609; e20 - HD 150862; e21 - HD 188985; e22 - HD 210709; e23 - HD 210910; e24 - HD 222349; e25 - BD+18 5215; e26 - HD 223938. Full table is only available in electronic form.

ion	λ	χ_{ex}	$\log gf$	e1	e2	e3	e4	e5	e6	e7	e8	e9	e10...
Fe I	4514.19	3.05	-2.050	89	24	76	34	79	36	67	87	24	32...
Fe I	4551.65	3.94	-2.060	48	5	41	12	45	...	31	50	7	...
Fe I	4554.46	2.86	-3.050	...	13	...	16
Fe I	4579.82	3.07	-2.830	47	...	41	...	36	...	25	9...
Fe I	4587.13	3.57	-1.780	83	26	79	27	80	34	61	86	23	34...
Fe I	4613.21	3.29	-1.670	87	...	95	46	91	62	73	93	33	47...
.
.

3.5. Metallicities and Microturbulent Velocities

Equivalent widths were measured with IRAF, and Fe I and Fe II lines with $10 < W_\lambda < 160 \text{ m}\text{\AA}$ were considered. Photospheric 1D models were extracted from the NMARCS grid (Plez et al. 1992), originally developed by Bell et al. (1976) and Gustafsson et al. (1975) for gravities $\log g < 3.3$. For less evolved stars, with $\log g \geq 3.3$ the models by Edvardsson et al. (1993) were adopted.

Table 4. Colours and magnitudes. V magnitudes are from the Hipparcos database, otherwise from SIMBAD (marked with *); K_s from 2MASS Point Source Catalog; B_1 , B_2 , V_1 and G are Geneva magnitudes; “H”: Hipparcos; “S”: SIMBAD; “L”: LNA. Uncertainties for Hipparcos database are of ± 0.01 whereas for SIMBAD they were estimated in ± 0.05 .

star	(B-V) _S	(B-V) _H	(B-V) _L	(V-I) _L	(V-R) _L	(R-I) _L	V	K_s	B_1	B_2	V_1	G
HD 749	1.130	1.126(12)	1.126	1.096	0.581	0.515	7.91	5.385(9)	
HR 107	0.430	0.447(5)	0.408	0.506	0.245	0.261	6.05	4.942(13)	0.992	1.401	1.172	1.525
HD 5424	1.130	1.141(2)	1.169	1.003	0.521	0.482	9.48	7.015(15)	1.372	1.117	0.283	0.466
HD 8270	0.490	0.537(17)	0.539	0.664	0.334	0.330	8.82	7.524(15)	1.013	1.352	1.063	1.390
HD 12392	1.060	...	1.126	0.842	0.460	0.382	8.49*	6.231(31)	
HD 13551	0.550	0.599(24)	0.522	0.682	0.351	0.331	9.32	...	1.014	1.363	1.076	1.420
HD 22589	0.710	...	0.752	0.806	0.419	0.387	8.97*	7.265(11)	
HD 27271	1.000	1.011(17)	1.028	1.051	0.542	0.509	7.53	5.270(11)	
HD 48565	0.528	0.562(22)	7.20	5.806(17)	1.007	1.355	1.028	1.352
HD 76225	0.510	0.567(22)	0.522	0.594	0.300	0.294	9.23	7.979(39)	1.017	1.359	1.058	1.390
HD 87080	0.780	0.775(12)	0.761	0.797	0.405	0.392	9.40	7.567(19)	1.120	1.275	0.769	1.050
HD 89948	0.500	0.545(11)	0.543	0.612	0.309	0.303	7.50	6.189(19)	1.036	1.338	1.021	1.347
HD 92545	0.470	0.503(3)	0.500	0.592	0.299	0.293	8.55	7.282(23)	1.016	1.362	1.080	1.412
HD 106191	0.680	...	0.600	0.643	0.323	0.320	10.00*	8.586(21)	1.053	1.330	0.966	1.284
HD 107574	0.400	0.441(8)	0.434	0.524	0.263	0.261	8.55	7.415(17)	0.983	1.384	1.153	1.505
HD 116869	0.970	1.040(15)	1.041	0.997	0.520	0.477	9.49	7.143(19)	
HD 123396	1.180	1.190(15)	1.224	1.178	0.598	0.580	8.97	6.144(17)	
HD 123585	0.520	0.519(12)	0.505	0.555	0.285	0.270	9.28	8.081(19)	1.015	1.362	1.061	1.405
HD 147609	0.470	0.600(15)	0.584	0.655	0.332	0.323	8.57	...	1.010	1.359	1.078	1.421
HD 150862	0.490	...	0.515	0.578	0.296	0.282	9.17*	8.009(27)	1.020	1.355	1.068	1.399
HD 188985	0.480	0.532(17)	0.550	0.604	0.300	0.304	8.55	7.231(23)	1.034	1.345	1.019	1.347
HD 210709	1.060	1.103(5)	1.117	1.051	0.559	0.492	9.23	6.711(19)	
HD 210910	1.100	1.100(30)	1.086	1.133	0.596	0.537	8.49	5.857(19)	1.307	1.144	0.344	0.513
HD 222349	0.500	...	0.495	0.571	0.287	0.284	9.20*	7.940(25)	1.001	1.365	1.082	1.421
BD+18 5215	0.370	9.74*	8.535(11)	0.991	1.368	1.110	1.452
HD 223938	0.890	0.905(14)	0.873	0.893	0.461	0.432	8.62	6.504(13)	

Microturbulent velocities v_t were determined by canceling the trend of Fe I abundance vs. equivalent width.

The uncertainties on the metallicity are due to uncertainties on the input parameters: temperature, $\log g$ and microturbulent velocity. The variation of these parameters affects the iron abundance $\epsilon(\text{Fe})$, as follows

$$\sigma_{\epsilon(\text{Fe})} = \sqrt{(\Delta\epsilon(\text{Fe})_T)^2 + (\Delta\epsilon(\text{Fe})_{lg})^2 + (\Delta\epsilon(\text{Fe})_v)^2} \quad (3)$$

where $\Delta\epsilon(\text{Fe})_T$, $\Delta\epsilon(\text{Fe})_{lg}$ and $\Delta\epsilon(\text{Fe})_v$ are the differences on the iron abundances due to variations on temperature, $\log g$ and microturbulent velocity, respectively.

The contributions of the equivalent widths (from 0.5 to 0.9 mÅ) to the uncertainty in metallicity are negligible (Cayrel 1989), where uncertainties on continuum placement are not taken into account.

For HD 5424, a variation of $\Delta T = 100$ K in the temperature results in $\Delta\epsilon(\text{Fe})_T = 1.940 \times 10^6$, $\Delta \log g = 0.3$ dex in $\log g$ results in $\Delta\epsilon(\text{Fe})_{lg} = 2.855 \times 10^6$ and $\Delta v_t = 0.1$ km/s in v_t results in $\Delta\epsilon(\text{Fe})_v = 0.803 \times 10^6$ in the $\epsilon(\text{Fe})$. For HD 150862, $\Delta\epsilon(\text{Fe})_T = 5.65 \times 10^5$ for $\Delta T = 100$ K, $\Delta\epsilon(\text{Fe})_{lg} = 1.69 \times 10^6$ for $\Delta \log g = 0.1$ dex and $\Delta\epsilon(\text{Fe})_v = 0.113 \times 10^6$ for $\Delta v_t = 0.1$ km/s. The quantity of interest is the logarithm of $\epsilon(\text{Fe})$, such that $\sigma_{\log \epsilon(\text{Fe})} = (\sigma_{\epsilon(\text{Fe})})/(\epsilon(\text{Fe}) \ln 10)$. Consequently, $\sigma_{[\text{Fe}/\text{H}]} = \sqrt{\sigma_{\log \epsilon(\text{Fe})}^2 + \sigma_{\log \epsilon(\text{Fe})_{\odot}}^2}$, resulting $\sigma_{[\text{Fe}/\text{H}]} = 0.18$ for HD 5424, and this result should be typical for all sample stars with $\log g <$

3.3. For HD 150862, $\sigma_{[\text{Fe}/\text{H}]} = 0.04$, this uncertainty being adopted for stars with $\log g \geq 3.3$.

3.6. Adopted Atmospheric Parameters

The atmospheric parameters were derived in an iterative way, adopting initial values of $\log g$ and $[\text{Fe}/\text{H}]$ according to North et al. (1994) and Gómez et al. (1997). The lines of Fe I and Fe II were used separately in order to test the ionization equilibrium (see Sect. 3.3). In this first iteration, one searches for values of $\log g$, $[\text{Fe}/\text{H}]$ and v_t corresponding to the ionization equilibrium in order to verify the trend of the results. Using the average of the temperatures and masses from isochrones, the surface gravity was determined from equation 1, in order to be compared with that from the ionization equilibrium.

In the first iteration, values different from the ones adopted initially for $[\text{Fe}/\text{H}]$ and $\log g$ from equation 1 were obtained. In this case, these new values were used as input in the colour-temperature calibrations and the procedure was restarted. The procedure was repeated until the input parameters matched the output ones, providing a consistent set of atmospheric parameters. After several iterations, it was possible to define a set of atmospheric parameters for each star, shown in Table 9. These results indicate that our sample contains giants, subgiants and dwarfs. Table 11 shows atmospheric parameters for barium stars found in the literature.

Table 7. Temperatures based on calibrations by Alonso et al. (1996) or Alonso et al. (1999) and for the Geneva system those by Meléndez & Ramírez (2003) for subgiants or dwarfs and Ramírez & Meléndez (2004) for giants.

star	$T_{(B-V)S}$	$T_{(B-V)H}$	$T_{(B-V)L}$	$T_{(V-I)L}$	$T_{(V-R)L}$	$T_{(R-I)L}$	$T_{(V-K)}$	T_{B2-V1}	T_{B2-G}	T_{B1-B2}
HD 749	4570	4570	4570	4530	4570	4570	4590
HR 107	6440	6370	6540	6460	6600	6180	6410	6410	6430	6360
HD 5424	4430	4410	4360	4720	4740	4690	4620	4400	4470	4460
HD 8270	6130	5940	5940	5760	5860	5650	6080	6050	6050	6050
HD 12392	4670	...	4560	5110	5010	5190	4840
HD 13551	5890	5730	6000	5700	5740	5640	...	6060	6120	6130
HD 22589	5420	...	5290	5320	5370	5300	5470
HD 27271	4950	4930	4890	4700	4780	4690	4940
HD 48565	5910	5790	5920	5820	5860	5820
HD 76225	6150	5930	6110	6110	6180	5970	6210	6070	6110	6080
HD 87080	5280	5290	5330	5510	5560	5480	5450	5250	5370	5370
HD 89948	6150	5970	5980	5970	6070	5820	6060	5950	5990	6000
HD 92545	6390	6250	6260	6130	6240	5950	6190	6220	6240	6200
HD 106191	5550	...	5820	5870	6000	5720	5920	5780	5850	5830
HD 107574	6520	6330	6360	6450	6440	6330	6430	6370	6380	6370
HD 116869	4760	4620	4620	4740	4750	4710	4740
HD 123396	4230	4220	4160	4430	4480	4360	4360
HD 123585	6160	6170	6220	6470	6400	6430	6460	6140	6220	6240
HD 147609	6400	5880	5940	5800	5950	5620	...	6210	6280	6210
HD 150862	6350	...	6240	6280	6310	6150	6460	6260	6280	6270
HD 188985	6300	6080	6010	6090	6210	5910	6120	5960	6020	6020
HD 210709	4670	4600	4570	4620	4630	4660	4590
HD 210910	4660	4660	4680	4480	4540	4510	4520	4520	4570	4430
HD 222349	6020	...	6040	6150	6190	6040	6140	6040	6060	6070
BD+18 5215	6670	6310	6270	6280	6280
HD 223938	4930	4900	4970	4980	4990	4920	4990

The use of models by Gustafsson et al. (1975) led to $\Delta[\text{FeI}/\text{H}]$ and $\Delta[\text{FeII}/\text{H}] \leq 0.03$ dex relative to models by Edvardsson et al. (1993) and Plez et al. (1992) for most stars. For two stars, $\Delta[\text{Fe}/\text{H}] \approx 0.15$ dex and for another 4 ones, 0.04 dex $< \Delta[\text{Fe}/\text{H}] < 0.09$ dex.

In Table 10 are given the bolometric corrections $BC(V)$ determined according to Alonso et al. (1995) for dwarfs and subgiants and to Alonso et al. (1999) for giants, with good agreement with values determined from a linear interpolation on Lejeune et al. (1998) grids. The uncertainties on $BC(V)$ were estimated by computing how the uncertainties on temperatures modify its value; from equations 4 to 12, one obtains the absolute magnitude M_v , the bolometric magnitude M_{bol} , the luminosity (L_*/L_\odot), the radius (R_*/R_\odot) and the mass (M_*/M_\odot), providing as input the distance $D(\text{pc})$, A_v , V and $\log g$:

$$M_v = V - 5 \log D + 5 - A_v \quad (4)$$

$$\sigma_{M_v} = \left[(\sigma_V)^2 + \left(\frac{5\sigma_D}{D \ln(10)} \right)^2 + \sigma_{A_v}^2 \right]^{0.5} \quad (5)$$

$$M_{bol*} = M_v + BC(V) \quad (6)$$

$$\sigma_{M_{bol*}} = \left(\sigma_{M_v}^2 + \sigma_{BC}^2 \right)^{0.5} \quad (7)$$

$$L_* = 10^{-0.4(M_{bol*} - M_{bol\odot})} L_\odot \quad (8)$$

$$\sigma_L = L_{\odot} 0.4 \ln(10) \left(\sigma_{M_{bol*}}^2 + \sigma_{M_{bol\odot}}^2 \right)^{0.5} \quad (9)$$

$$R_* = \left(\frac{L_* T_{eff\odot}^4}{L_\odot T_{eff*}^4} \right)^{0.5} R_\odot \quad (10)$$

$$\sigma_R = R \left[\left(\frac{\sigma_L}{2L} \right)^2 + \left(\frac{2\sigma_{T_{eff\odot}}}{T_{eff\odot}} \right)^2 + \left(\frac{2\sigma_{T_{eff*}}}{T_{eff*}} \right)^2 \right]^{0.5} \quad (11)$$

Recalling that $g = 10^{\log(g)}$ and $\sigma_g = g \ln(10) \sigma_{\log(g)}$

$$M_* = \frac{g_* R_*^2}{g_\odot R_\odot^2} M_\odot \quad (12)$$

$$\sigma_M = M \left[\left(\frac{\sigma_{g*}}{g*} \right)^2 + \left(\frac{\sigma_{g\odot}}{g\odot} \right)^2 + \left(\frac{2\sigma_R}{R} \right)^2 \right]^{0.5} \quad (13)$$

For masses computed with equation 12 and $\log g$ from ionization equilibrium, the results are those shown in column 8 of Table 10. These masses are lower than those derived from the isochrones (column 9), resulting in higher values for $\log g$ computed from equation 1.

Our derivations are essentially compatible with Mennessier et al. (1997) masses for barium stars, according to their luminosity classes: 1 - 1.6 M_\odot for dwarfs, and 1 - 3 M_\odot for giants and subgiants.

For stars with no Hipparcos parallaxes, distances also had to be derived iteratively. In the cases where extinction was null,

Table 6. Temperatures based on Lejeune et al. (1998) calibrations.

star	$T_{(B-V)S}$	$T_{(B-V)H}$	$T_{(B-V)L}$	$T_{(V-I)L}$	$T_{(V-R)L}$	$T_{(R-I)L}$	$T_{(V-K)}$
HD 749	4700	4710	4770	4570	4590	4540	4620
HR 107	6480	6400	6630	6450	6540	6370	6460
HD 5424	4550	4520	4530	4690	4660	4700	4650
HD 8270	6160	5960	5990	5870	5880	5860	6200
HD 12392	4690	...	4610	5230	5100	5430	4870
HD 13551	5890	5720	6030	5800	5760	5850	...
HD 22589	5460	...	5390	5420	5380	5480	5600
HD 27271	5010	4990	5010	4700	4800	4630	4950
HD 48565	5930	5760	6080
HD 76225	6170	5930	6150	6180	6170	6180	6310
HD 87080	5360	5370	5440	5630	5600	5680	5400
HD 89948	6160	5970	6010	6060	6060	6050	6180
HD 92545	6440	6290	6350	6200	6220	6180	6270
HD 106191	5570	...	5860	5970	6000	5940	6050
HD 107574	6550	6340	6410	6420	6390	6450	6460
HD 116869	4910	4780	4820	4680	4690	4660	4760
HD 123396	4410	4350	4310	4440	4450	4430	4380
HD 123585	6210	6220	6330	6460	6390	6560	6500
HD 147609	6450	5890	6000	5920	5970	5870	...
HD 150862	6410	...	6340	6330	6300	6370	6500
HD 188985	6360	6120	6080	6170	6210	6140	6250
HD 210709	4780	4690	4720	4620	4620	4610	4620
HD 210910	4740	4740	4830	4520	4540	4500	4550
HD 222349	6040	...	6100	6220	6190	6240	6270
BD+18 5215	6800	6400
HD 223938	5000	4970	5080	4940	4980	4890	5000

the determination of the colours was straight forward, the temperatures and the other parameters, $\log g$, $[\text{Fe}/\text{H}]$ and BC. The distance can be determined by setting the mass. In the case of extinction variation on which an average of A_V was adopted, the distance obtained can be different from that used by computing A_V . In this case, the new distance was used to restart the procedure, computing new A_V , colours and temperatures. The procedure was repeated until the output distance matched the input one. In both cases, the calculation was made for several masses inside the range given by Mennessier et al. (1997) and the absolute magnitudes were used to derive the masses from isochrones in order to be compared with the input masses. The $\log g$ was obtained with equation 1. The mass chosen was that for which $\log g$ from the equation 1 was inside the range of 0.3 dex of the spectroscopic one. Once the mass was set, the distances were recalculated, as shown in Table 8.

According to Thévenin & Idiart (1999), the NLTE affects Fe I lines more than Fe II ones, and it directly affects the $\log g$ derived from ionization equilibrium. For this reason, the gravities adopted were those resulting from expression 1, whereas for the metallicities, Fe II lines were used, as shown in column 7 of Table 9. It is worth noting that using the gf-values for Fe II lines by Meléndez & Barbuy (2006), the abundances of Fe derived from the Fe I and Fe II lines are closer to each other and the $\log g$ from ionization equilibrium increases by 0.2 dex relative to the case of the gf-values from NIST.

Table 9 compared with Table 11, shows that differences are stronger for HD 27271 and HD 147609. Temperatures derived

Table 8. Masses and distances adopted for stars with no Hipparcos parallax π_H values.

star	$D_{\min}-D_{\max}$	$M_{\min}-M_{\max}$	adopted
HD 12392	150-240pc	1.6-2.4 M_{\odot}	219(30)pc 2.0(1) M_{\odot}
HD 22589	240-288pc	1.6-1.8 M_{\odot}	249(20)pc 1.6(1) M_{\odot}
HD 106191	140-180pc	1.0-1.1 M_{\odot}	145(20)pc 1.0(1) M_{\odot}
HD 150862	70-90pc	1.0-1.2 M_{\odot}	74(10)pc 1.1(1) M_{\odot}
HD 222349	154-182pc	1.1-1.2 M_{\odot}	168(20)pc 1.2(1) M_{\odot}
BD+18 5215	140-190pc	1.1-1.2 M_{\odot}	153(20)pc 1.1(1) M_{\odot}

Table 9. Stellar parameter results. T_{eff} : photometric temperature; T_{exc} : excitation temperature; $\log g(\text{C})$: $\log g$ related to curve of growth; $\log g(\text{D})$: $\log g$ related to masses from isochrones. Numbers in parenthesis are errors in last decimals.

star	T_{eff}	T_{exc}	$\log g(\text{C})$	$\log g(\text{D})$	$[\text{Fe I}/\text{H}]$	$[\text{Fe II}/\text{H}]$	v_t
HD 749	4610	4580	2.3	2.8(1)	-0.06	+0.17	0.9
HR 107	6440	6650	4.0	4.08(7)	-0.34	-0.36	1.6
HD 5424	4570	4700	1.8	2.0(3)	-0.51	-0.55	1.1
HD 8270	5940	6070	4.2	4.2(1)	-0.44	-0.42	0.9
HD 12392	5000	5000	3.2	3.2(1)	-0.06	-0.12	1.2
HD 13551	5870	6050	3.7	4.0(1)	-0.44	-0.24	1.1
HD 22589	5400	5630	3.3	3.3(1)	-0.12	-0.27	1.1
HD 27271	4830	4830	2.3	2.9(1)	-0.09	+0.17	1.3
HD 48565	5860	6050	3.8	4.01(8)	-0.71	-0.62	1.0
HD 76225	6110	6330	3.7	3.8(1)	-0.34	-0.31	1.4
HD 87080	5460	5550	3.7	3.7(2)	-0.49	-0.44	1.0
HD 89948	6010	6010	4.2	4.30(8)	-0.28	-0.30	1.2
HD 92545	6210	6270	4.0	4.0(1)	-0.15	-0.12	1.3
HD 106191	5890	5890	4.2	4.2(1)	-0.22	-0.29	1.1
HD 107574	6400	6400	3.6	3.6(2)	-0.56	-0.55	1.6
HD 116869	4720	4850	2.1	2.2(2)	-0.35	-0.32	1.3
HD 123396	4360	4480	1.2	1.4(3)	-1.19	-0.99	1.2
HD 123585	6350	6450	4.2	4.2(1)	-0.44	-0.48	1.7
HD 147609	5960	5960	3.3	4.42(9)	-0.45	+0.08	1.5
HD 150862	6310	6310	4.6	4.6(1)	-0.11	-0.10	1.4
HD 188985	6090	6190	4.3	4.3(1)	-0.25	-0.30	1.1
HD 210709	4630	4680	2.3	2.4(2)	-0.07	-0.04	1.1
HD 210910	4570	4770	2.0	2.7(2)	-0.37	+0.04	2.0
HD 222349	6130	6190	3.9	3.9(1)	-0.58	-0.63	1.1
BD+18 5215	6300	6300	4.2	4.2(1)	-0.44	-0.53	1.5
HD 223938	4970	5150	2.7	3.1(1)	-0.35	-0.13	1.0

from the colours indices in the present work for HD 27271 and HD 147609 are lower than those found in the literature. Furthermore, the metallicities used were those derived from Fe II lines instead of ionization equilibrium. Also the masses derived using $\log g$ from ionization equilibrium are very small (see column 8 of Table 10), therefore we preferred to use $\log g$ derived by using masses from isochrones, and Fe II lines for the determination of metallicities.

4. Abundances

The LTE abundance analysis and the spectrum synthesis calculations were performed using the codes by Spite (1967, and

Table 10. Bolometric corrections, absolute magnitudes, luminosities, radii and masses for the sample stars. $BC_a(V)$: bolometric corrections using Alonso et al. (1996) for dwarfs and subgiants and Alonso et al. (1999) for giants; $BC_l(V)$: bolometric corrections using Lejeune et al. (1998); M_*/M_\odot : stellar masses from curve of growth; M_i/M_\odot : stellar masses from isochrones. Numbers in parenthesis are errors in last decimals.

star	$BC_a(V)$	$BC_l(V)$	M_v	M_{bol}	L_*/L_\odot	R_*/R_\odot	M_*/M_\odot	M_i/M_\odot
HD 749	-0.43(6)	-0.47(7)	1.9(3)	1.4(3)	21(6)	7(1)	0.4(1)	1.2
HR 107	-0.08(1)	-0.04(1)	3.3(1)	3.2(1)	4.2(5)	1.6(1)	1.0(3)	1.2
HD 5424	-0.44(6)	-0.48(7)	-0.5(8)	-0.9(8)	184(130)	22(8)	1.1(8)	1.9
HD 8270	-0.13(1)	-0.12(1)	4.4(2)	4.2(2)	1.6(3)	1.2(1)	0.8(3)	0.9
HD 12392	-0.26(3)	-0.28(2)	1.8(3)	1.5(3)	20(6)	6.0(9)	2.0(8)	2.0
HD 13551	-0.14(1)	-0.12(1)	4.0(2)	3.8(2)	2.3(5)	1.5(2)	0.4(1)	0.9
HD 22589	-0.20(2)	-0.19(2)	2.0(3)	1.8(3)	16(4)	4.5(6)	1.4(5)	1.6
HD 27271	-0.32(4)	-0.35(5)	1.3(2)	1.0(2)	32(7)	8(1)	0.5(2)	1.9
HD 48565	-0.15(1)	-0.14(1)	3.9(1)	3.7(1)	2.5(3)	1.5(1)	0.5(1)	0.9
HD 76225	-0.08(1)	-0.09(1)	2.6(3)	2.5(3)	8(2)	2.5(4)	1.1(5)	1.4
HD 87080	-0.20(2)	-0.19(2)	3.2(4)	3.0(4)	5(2)	2.5(5)	1.1(3)	1.2
HD 89948	-0.11(1)	-0.10(1)	4.3(1)	4.2(1)	1.6(2)	1.18(9)	0.8(2)	1.0
HD 92545	-0.08(1)	-0.06(1)	3.1(3)	3.0(3)	5(1)	1.9(2)	1.3(5)	1.3
HD 106191	-0.11(1)	-0.11(1)	4.2(3)	4.0(3)	1.9(6)	1.3(2)	1.0(4)	1.0
HD 107574	-0.08(1)	-0.06(1)	2.0(5)	1.9(5)	13(6)	3.0(6)	1.3(6)	1.4
HD 116869	-0.37(4)	-0.38(5)	0.2(5)	-0.1(5)	88(40)	14(4)	0.9(5)	1.2
HD 123396	-0.57(7)	-0.61(7)	-0.7(8)	-1.3(8)	255(180)	28(10)	0.4(3)	0.8
HD 123585	-0.10(4)	-0.06(1)	3.7(2)	3.6(2)	2.8(6)	1.4(2)	1.1(4)	1.1
HD 147609	-0.10(1)	-0.09(1)	4.7(2)	4.6(2)	1.2(2)	1.02(9)	0.07(2)	1.0
HD 150862	-0.07(1)	-0.06(1)	4.7(3)	4.7(3)	1.1(3)	0.9(1)	1.1(4)	1.1
HD 188985	-0.10(1)	-0.09(1)	4.1(2)	4.0(2)	1.9(4)	1.2(1)	1.1(2)	1.1
HD 210709	-0.53(6)	-0.45(7)	1.1(4)	0.5(4)	48(20)	11(2)	0.8(4)	1.1
HD 210910	-0.45(6)	-0.50(7)	2.0(4)	1.6(4)	19(6)	7(1)	0.2(1)	1.0
HD 222349	-0.12(1)	-0.11(1)	3.1(2)	2.9(2)	5(1)	2.0(2)	1.2(4)	1.2
BD+18 5215	-0.10(1)	-0.08(1)	3.8(3)	3.7(3)	3(1)	1.4(2)	1.1(4)	1.1
HD 223938	-0.31(4)	-0.28(2)	1.9(4)	1.6(4)	18(6)	6(1)	0.6(2)	1.4

subsequent improvements in the last thirty years), described in Cayrel et al. (1991) and Barbuy et al. (2003).

Table 15 shows the resulting abundances ($\log \epsilon(X)$ and $[X/Fe]$) for all atomic lines, whereas Tables 16 and 17 show the mean abundance of each element, obtained for the 26 sample barium stars. Figures 11 to 14 show $[X/Fe]$ vs. $[Fe/H]$. For most elements, the solar abundances used were extracted from Grevesse & Sauval (1998), otherwise references are indicated in Table 17.

For the stars HD 749, HD 13551, HD 27271, HD 123396, HD 147609, HD 210910 and HD 223938, the difference between the metallicities derived from Fe I and Fe II lines, $\Delta[Fe/H] = [Fe II/H] - [Fe I/H] \geq 0.2$ dex (see Table 9). There are several possible explanations for it, such as the NLTE effect in lines of Fe I, imprecision in stellar parameters (T_{eff} , $\log g$, v_t), blends in Fe I and Fe II lines. Simmerer et al. (2004) also observed this effect in their sample of 159 giants and dwarfs. They established relations between $\Delta[Fe/H]$ and T_{eff} or $\log g$ and, despite having a dispersion, it is possible to note that the differences seem to be larger at lower temperatures. Kraft & Ivans (2003) attributed this effect to an inadequacy of model atmospheres. Yong et al. (2003) observed a similar behaviour in the relation between $\Delta[Fe/H]$ and T_{eff} for giants of the metal-poor globular cluster NGC 6752, also becoming more pronounced for the cooler stars.

For the 7 stars mentioned before, the resulting $[X/Fe]$ were very low, as shown by the starred symbols of Figures 11 to 14, and for this reason, the abundances were also determined by using metallicities from Fe I lines, as shown in Figures 11 to 14 and Tables 15, 16 and 17, and they were used in Figures 4,

Table 11. Atmospheric parameters for barium stars collected in the literature. References: E93: Edvardsson et al. (1993); G96: Gratton et al. (1996); T99: Thévenin & Idiart (1999); P05: Pereira (2005); P03: Pereira & Junqueira (2003); B92: Barbuy et al. (1992); N94: North et al. (1994); S86: Smith & Lambert (1986); L91: Luck & Bond (1991); S93: Smith et al. (1993). Numbers in parenthesis are errors in last decimals.

star	$T_{eff}(K)$	$\log g$	[M/H]	$v_t(km/s)$	ref
HR 107	6488	4.08	-0.37	-	E93
HR 107	6431	4.06	-0.37	1.98	G96
HR 107	6462	4.17	-0.21	1.00	T99
HD 8270	6100	4.2	-0.53	1.4	P05
HD 13551	6400	4.4	-0.28	1.6	P05
HD 22589	5600	3.8	-0.16	1.4	P05
HD 27271	5350	2.30	-0.50	3.0	B92
HD 48565	5910	3.50	-0.90	1.2(2)	N94
HD 48565	5929	3.72	-0.54	1.00	T99
HD 76225	6010	3.50	-0.50	1.7(2)	N94
HD 87080	5600	4.00	-0.51	1.2	P03
HD 89948	5929	4.10	-0.31	1.00	S86
HD 89948	6000	4.00	-0.13	1.80	L91
HD 89948	5950	4.10	-0.27	0.80	S93
HD 92545	6240	3.90	-0.33	1.7(1)	N94
HD 106191	5840	4.05	-0.40	1.0(1)	N94
HD 107574	6340	3.63	-0.80	1.9(3)	N94
HD 123585	6047	3.50	-0.50	1.8(3)	N94
HD 123585	6000	3.50	-0.50	2.00	L91
HD 147609	6270	3.50	-0.50	1.2(2)	N94
HD 147609	6300	3.61	-0.36	1.20	T99
HD 150862	6135	4.05	-0.30	1.2(1)	N94
HD 150862	6200	4.00	-0.22	2.20	L91
HD 188985	5960	3.78	-0.30	1.4(1)	N94
HD 222349	6000	3.76	-0.90	1.8	N94
BD+18 5215	6290	4.49	-0.50	1.2(2)	N94

5, 6, 9, 10, 15, 16, 17, 18. For the remaining stars, abundances in these figures were obtained using metallicities derived from Fe II lines.

The abundance results of the sample stars are essentially homogeneous, even considering the different luminosity classes, as shown in Figures 11 to 14. Regarding Al, Na, α - and iron peak elements, the behaviour of $[X/Fe]$ vs. $[Fe/H]$ is in agreement with disk stars. For heavy elements, there is a variation that could be explained by the amount of enriched material that each star received from the more evolved companion. The sample is too small to reveal differences between the 4 halo stars and the disk ones. The overabundance found for the s-elements in the sample stars is expected for barium stars and this peculiarity is independent of the luminosity class. Literature abundance data for the present sample barium stars are shown in Table 20.

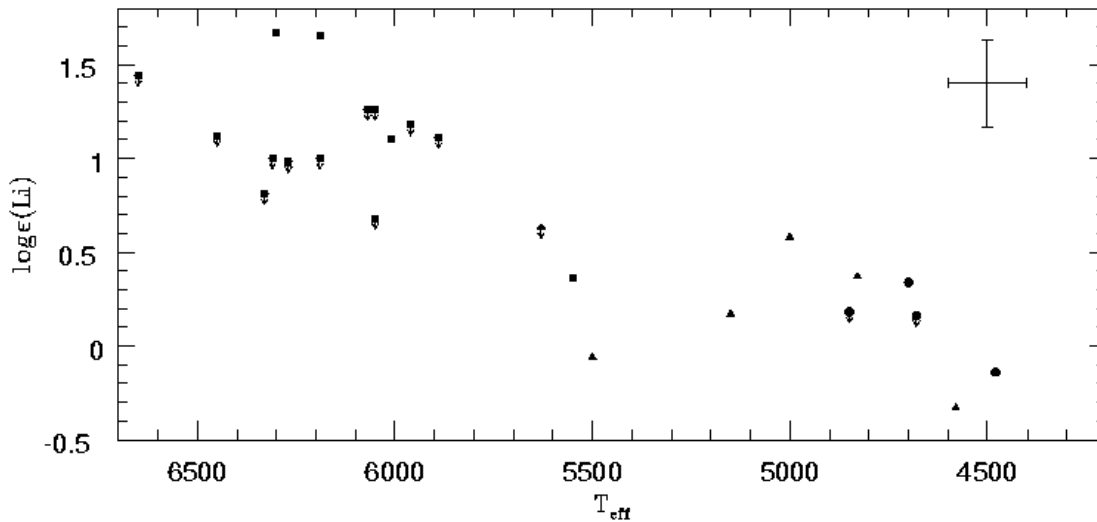


Fig. 4. Lithium abundance as a function of temperatures. Symbols: squares: dwarf stars ($\log g \geq 3.7$); triangles: subgiants ($2.4 < \log g < 3.7$); circles: giants ($\log g \leq 2.4$). The arrows indicate an upper limit.

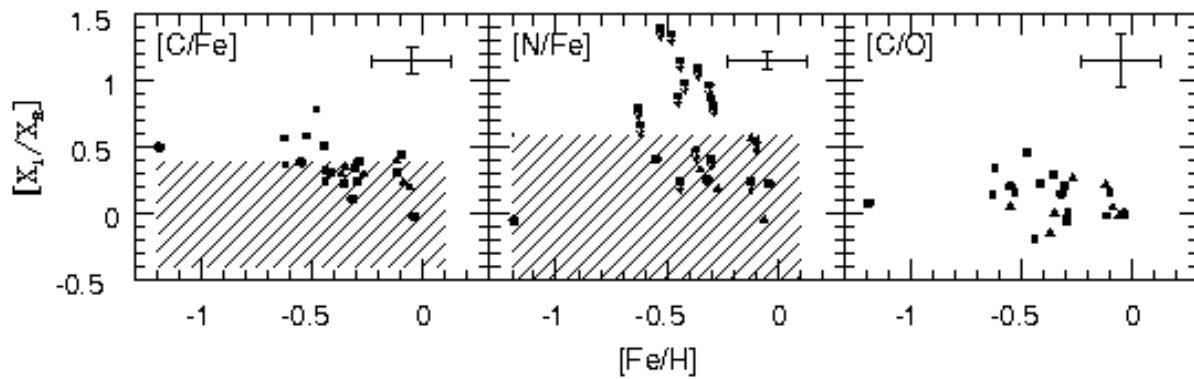


Fig. 5. [C,N/Fe] and [C/O] as a function of [Fe/H]. Symbols are the same as in Figure 4. The arrows indicate an upper limit. In the dashed region are the disk and halo stars of Goswami & Prantzos (2000).

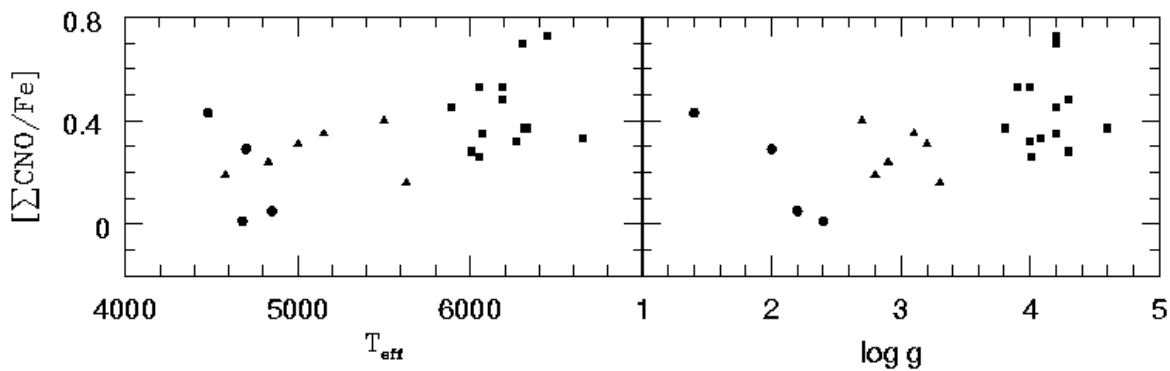


Fig. 6. $[\Sigma\text{CNO}/\text{Fe}]$ as a function of T_{eff} or $\log g$. Symbols are the same as in Figure 4.

4.1. Lithium

Lithium is among the yields of primordial nucleosynthesis. It can also be produced in stars with $M \leq 8 M_{\odot}$, through spallation by cosmic rays (Woosley & Weaver 1995) and the ν -process suggested for the first time by Domogatskii et al. (1977) and later by Woosley et al. (1990) and Timmes et al.

(1995). Red Giant Branch or Asymptotic Giant Branch stars possibly produce Li (Sackmann & Boothroyd 1992, 1999) and some of them become Lithium Rich Giants (Brown et al. 1989; Castilho et al. 1998). However, Li is mainly destroyed during the life of a star, and for this reason, it can be used as an appraiser of its age. Cooler stars have a deeper convective zone,

Table 12. Derived abundances of Li, C and N. The stars codes in the header are: e1 - HD 749; e2 - HR 107*; e3 - HD 5424; e4 - HD8270*; e5 - 12392; e6 - 13551*; e7 - HD 22589; e8 - HD 27271; e9 - HD 48565*; e10 - HD 76225*; e11 - HD 87080*; e12 - HD 89948*; e13 - HD 92545*; e14 - HD 106191*; e15 - HD 107574*; e16 - HD 116869; e17 - HD 123396; e18 - HD 123585*; e19 - HD 147609*; e20 - HD 150862*; e21 - HD 188985; e22 - HD 210709; e23 - HD 210910*; e24 - HD 222349*; e25 - BD+18 5215*; e26 - HD 223938. The G band covers the region $\lambda\lambda 4295 - 4315 \text{ \AA}$. The stars with '*' show an upper limit for N.

el	mol	λ	e1	e2	e3	e4	e5	e6	e7	e8	e9	e10	e11	e12	e13	e14	e15	e16	e17	e18	e19	e20	e21	e22	e23	e24	e25	e26	
Li	...	6707.776	-0.33	<1.44	0.10	<1.08	0.58	<1.36	<0.63	0.37	<0.68	<0.94	0.36	1.10	<0.98	<1.11	...	<0.18	-0.14	<1.12	<1.18	<1.00	<1.00	<0.16	-0.06	1.47	1.67	0.17	
Li	...	6707.927	-0.33	<1.44	0.50	<1.38	0.58	<1.12	<0.63	0.37	<0.68	<0.63	0.36	1.10	<0.98	<1.11	...	<0.18	-0.14	<1.12	<1.18	<1.00	<1.00	<0.16	-0.06	1.77	1.67	0.17	
C	C ₂	5135.600	8.62	8.39	8.35	8.30	8.79	8.18	8.55	8.59	8.27	8.58	8.38	8.47	8.63	8.60	8.37	8.31	7.83	8.83	8.60	8.86	8.61	8.46	8.42	8.28	8.53	8.53	
C	C ₂	5165.254	8.67	8.39	8.35	8.40	8.84	8.28	8.55	8.69	8.27	8.58	8.40	8.47	8.68	8.60	8.37	8.31	7.83	8.83	8.60	8.86	8.61	8.46	8.52	8.48	8.53	8.53	
C	C ₂	5635.500	8.67	8.39	8.40	8.50	8.79	8.48	8.55	8.69	8.27	8.58	8.42	...	8.78	8.65	8.37	8.31	7.81	8.83	8.60	8.86	8.61	8.46	8.52	8.68	8.63	8.53	
C	CH	G band	8.67	8.39	8.35	8.40	8.79	8.28	8.55	8.69	8.27	8.47	8.42	8.47	8.78	8.65	8.32	8.31	7.83	8.83	8.50	8.86	8.61	8.46	8.32	8.28	8.63	8.53	
N	CN	6477.200	7.89	8.66	7.65	8.80	8.50	8.75	8.13	8.35	7.98	8.74	7.71	7.93	...	8.80	8.36	8.38	8.68	8.13	8.07	7.94	
N	CN	6478.400	...	8.66	7.65	...	8.30	9.15	7.63	8.35	7.88	8.74	7.71	7.83	...	8.80	8.36	8.38	8.68	8.13	8.07	
N	CN	6478.700	...	8.66	7.95	...	8.40	8.75	7.63	8.35	7.88	8.74	7.71	7.88	...	8.80	8.36	8.38	8.68	8.13	8.07	
N	CN	6479.000	8.09	8.66	8.15	8.75	7.88	8.74	7.71	8.08	...	8.36	8.38	8.68	8.13	8.07	
N	CN	6703.968	7.79	8.66	7.71	8.60	8.45	8.55	7.93	8.35	7.88	8.64	7.71	...	8.04	...	9.31	7.83	6.76	...	8.36	8.38	8.48	8.13	8.07	7.94	
N	CN	6706.733	7.79	8.66	7.71	8.60	8.40	8.55	7.93	8.35	7.88	8.64	7.71	...	8.04	...	9.31	7.83	6.76	...	8.36	8.38	8.48	8.13	8.07	7.94	
N	CN	6708.993	7.79	8.66	7.71	8.60	8.40	8.75	...	8.35	7.88	8.64	7.71	...	8.04	...	9.31	7.83	6.76	...	8.36	8.38	8.48	8.13	8.07	7.94	
N	CN	8030.410	7.74	...	7.71	8.40	8.30	8.25	7.83	8.15	7.78	8.44	7.71	8.10	8.04	8.77	9.31	7.73	6.51	8.80	8.36	8.38	8.58	8.13	7.97	8.79	7.84
N	CN	8030.720	7.79	...	7.81	8.40	8.40	...	7.83	8.25	7.78	8.14	7.81	8.10	8.04	8.47	9.21	7.93	6.75	8.80	8.36	8.38	8.18	8.13	7.97	8.79	7.94
N	CN	8034.970	7.79	...	7.75	7.90	8.30	7.55	7.78	8.35	7.78	7.94	7.71	7.85	8.04	8.07	...	7.93	6.66	8.08	7.88	8.13	7.97	8.09	8.79	7.84	
N	CN	8040.100	7.69	...	7.55	8.25	8.25	7.95	7.73	8.20	8.28	8.44	7.71	8.05	8.04	8.32	9.31	7.68	6.51	8.80	8.36	...	8.08	7.93	7.97	8.79	7.84
N	CN	8040.220	7.69	...	7.65	8.25	8.30	7.95	7.73	8.25	8.28	8.44	7.71	8.05	8.04	8.32	8.91	7.73	6.61	8.80	8.36	...	8.08	8.03	7.97	8.79	7.84

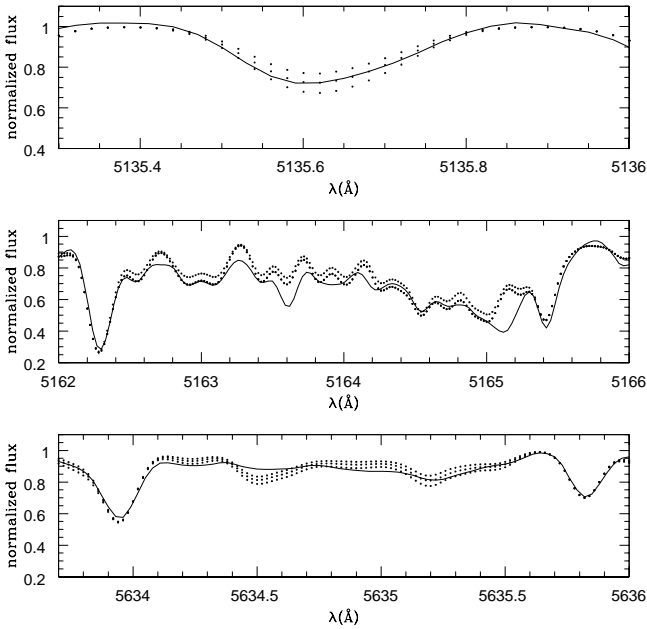


Fig. 7. Example of fits of the C₂ bands for the star HD 12392. Symbols: solid line: observed spectrum; dotted lines: synthetic spectra with several C abundances. Upper panel: $\log \epsilon(C) = 8.84, 8.79 \text{ e } 8.74$; Middle panel: $\log \epsilon(C) = 8.89, 8.84 \text{ e } 8.79$; Lower panel: $\log \epsilon(C) = 8.84, 8.79 \text{ e } 8.74$.

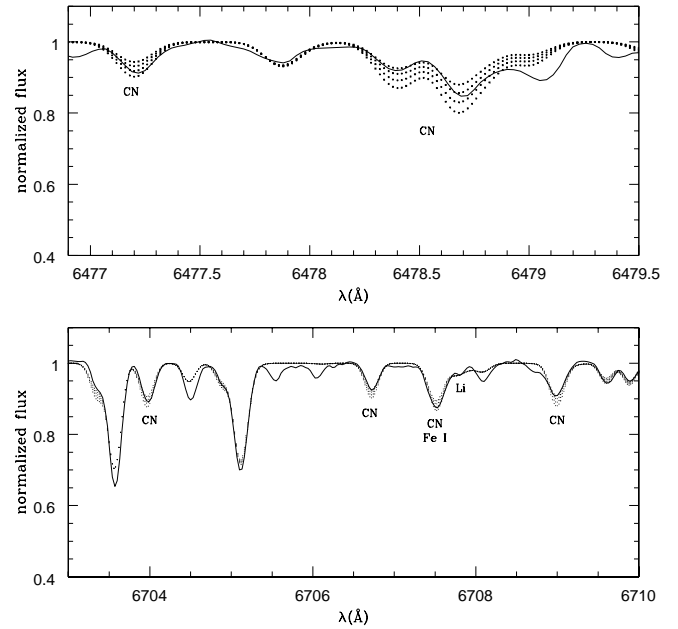


Fig. 8. Example of fits of CN bands for the star HD 12392. Symbols: solid line: observed spectrum; dotted lines: synthetic spectra with several N abundances. Upper panel: $\log \epsilon(N) = 8.60, 8.50, 8.40, 8.30$; Lower panel: $\log \epsilon(N) = 8.50, 8.45, 8.40, 8.35$.

consequently, Li is brought to inner regions where it is completely destroyed.

For low metallicity dwarfs there is an upper limit of the temperature where the convective zone acts such that surface Li can be preserved, forming the Spite's plateau (Spite & Spite 1982).

Castilho et al. (2000) showed that the globular cluster NGC 6397 presents a Li dilution curve where for $T_{\text{eff}} \approx 6000 \text{ K}$,

$\log \epsilon(\text{Li}) \approx 2.2$ and $T_{\text{eff}} \approx 4200 \text{ K}$, $\log \epsilon(\text{Li}) \approx -0.8$, indicating an additional Li destruction. Other causes for Li depletion have been suggested such as rotationally induced mixing and mass loss.

Most AGB stars rich in O and C are poor in Li (Boesgaard 1970; Denn et al. 1991; Kipper & Wallerstein 1990). Therefore, a barium star considered as a result of the mass transfer from the companion AGB should be also Li-poor.

Table 13. Average abundances from molecular lines and Li synthesis. '<' indicates an upper limit.

star	log ϵ (C)	[C/Fe]	log ϵ (N)	[N/Fe]	[C/O]	$[\Sigma\text{CNO}/\text{Fe}]$	log ϵ (Li)
HD 749	8.66	0.20	7.82	-0.04	-0.01±0.20	0.19	-0.33
HR 107	8.39	0.23	<8.66	<1.10	0.30±0.14	0.33	<1.44
HD 5424	8.36	0.39	7.78	0.41	0.21±0.20	0.29	0.34
HD 8270	8.41	0.31	<8.49	<0.99	0.23±0.14	0.35	<1.26
HD 12392	8.80	0.40	8.37	0.57	0.22±0.20	0.31	0.58
HD 13551	8.32	0.24	<8.64	<1.16	-0.19±0.14	0.53	<1.26
HD 22589	8.55	0.30	7.84	0.19	0.27±0.14	0.16	<0.63
HD 27271	8.67	0.24	8.31	0.48	0.05±0.20	0.24	0.37
HD 48565	8.27	0.37	<7.97	<0.67	0.34±0.14	0.26	<0.68
HD 76225	8.56	0.35	<8.58	<0.97	0.22±0.14	0.37	<0.81
HD 87080	8.41	0.33	<7.72	<0.24	0.36
HD 89948	8.47	0.25	<8.04	<0.42	-0.03±0.14	0.28	1.10
HD 92545	8.72	0.32	<8.04	<0.24	-0.01±0.14	0.32	<0.98
HD 106191	8.63	0.40	<8.45	<0.82	0.02±0.14	0.45	<1.11
HD 107574	8.36	0.39	<9.26	<1.89	0.06±0.14	0.94	...
HD 116869	8.31	0.11	7.86	0.26	0.15±0.20	0.05	<0.18
HD 123396	7.83	0.50	6.68	-0.05	0.08±0.20	0.43	-0.14
HD 123585	8.83	0.79	<8.80	<1.36	0.46±0.14	0.73	<1.12
HD 147609	8.58	0.51	<8.36	<0.89	<1.18
HD 150862	8.86	0.44	<8.36	<0.54	0.16±0.14	0.37	<1.00
HD 188985	8.61	0.39	8.49	0.87	-0.05±0.14	0.48	<1.00
HD 210709	8.46	-0.02	8.11	0.23	0.00±0.20	0.01	<0.16
HD 210910	8.45	0.30	<8.03	<0.48	-0.14±0.20	0.40	-0.06
HD 222349	8.46	0.57	<8.09	<0.80	0.14±0.14	0.53	1.65
BD+18 5215	8.58	0.59	<8.79	<1.40	0.16±0.14	0.70	1.67
HD 223938	8.53	0.36	7.90	0.33	0.01±0.20	0.35	0.17

The Li I lines at $\lambda 6708 \text{ \AA}$ in the present sample are very weak. For 14 of them it was possible to derive an upper limit for Li abundances. Table 13 shows the Li abundances and Figure 4 shows their behaviour with temperature. The abundances usually obtained for dwarfs are higher than for giants, even taking into account that in several cases it was possible to compute only an upper limit. For the dwarf star BD+18 5215, $T_{\text{eff}} = 6300 \text{ K}$ and $\log \epsilon(\text{Li}) = 1.67$ and for the coolest star in the sample HD 123396, $T_{\text{eff}} = 4360 \text{ K}$ and $\log \epsilon(\text{Li}) = -0.14$.

4.2. Carbon

C abundances were derived using molecular synthesis of the C_2 Swan (0,0) $\lambda 5165.2 \text{ \AA}$, C_2 Swan (0,1) $\lambda 5635.5 \text{ \AA}$ band heads and the G band ($\text{CH A}^3\Delta - \text{X}^3\pi$) at $\lambda 4290\text{-}4315 \text{ \AA}$. Examples of spectrum synthesis are shown in Figure 7.

Figure 5 shows that the sample stars are C-rich as compared with normal stars of the disk and halo, this being characteristic of barium stars (Bidelman & Keenan 1951; Warner 1965). Despite the dispersion, the results show an increasing trend in [C/Fe] toward lower metallicities, except for the halo giant HD 123396.

Barbuy et al. (1992) derived abundances of C, N and O for a sample of barium stars, including the star HD 27271 in common with the present sample. Through the synthesis of the C_2 line at $\lambda 5136 \text{ \AA}$, they found [C/Fe] = 0.15, compatible with the present work, [C/Fe] = 0.23, that is an average of several lines. They obtained the range $-0.25 \leq [\text{C}/\text{Fe}] \leq 0.3$ taking into account all stars in their sample and all indicators, and only 3 stars could be deficient in C. For the present sample the range $-0.02 \leq [\text{C}/\text{Fe}] \leq 0.79$ was found, with [C/Fe] < 0 for one star. Pereira (2005) determined C abundances for the stars HD 8270,

HD 13551 and HD 22589 from C I lines at $\lambda 5380 \text{ \AA}$, $\lambda 7113 \text{ \AA}$, $\lambda 7115 \text{ \AA}$, $\lambda 7117 \text{ \AA}$, $\lambda 7120 \text{ \AA}$, and found, respectively, [C/Fe] = 0.71, 0.46, 0.64 (see Table 20), which values are higher than the present analysis for the same stars (0.31, 0.24, 0.30, Table 13). For the star HD 87080, Pereira & Junqueira (2003) found [C I/Fe] = 0.61, also higher than in this work (0.33), but it is well known that the triplet at $\lambda 7115 - \lambda 7120 \text{ \AA}$ used by them is subject to strong NLTE effects (Przybilla et al. 2001). Comparing the results of [C/Fe] by North et al. (1994) with the stars in common with the present sample shown in Tables 20 and 13, a good agreement is seen, though their results for the stars HD 48565, HD 76225 and HD 107574 are higher. Their results are in the range $-0.15 \leq [\text{C}/\text{Fe}] \leq 0.89$, confirming the good agreement.

Figure 5 shows a decreasing trend of [C/Fe] toward higher metallicities for the sample barium stars. Reddy et al. (2003) found similar behaviour for their sample of F and G disk dwarfs, whereas Goswami & Prantzos (2000) found a constant behaviour centered in [C/Fe] ~ 0 for their sample of halo and disk stars, in the ranges $-0.4 < [\text{C}/\text{Fe}] < +0.4$ and $-1 < [\text{Fe}/\text{H}] < 0$. It is also possible to note that even the metal-poor barium stars are richer in C than normal stars of similar metallicities. The star HD 123396 does not follow the decreasing trend of [C/Fe] of Figure 5, and, if it is a halo giant, then it is C-rich relative to most stars of the halo and instead compatible with C-rich halo stars (Rossi et al. 2005). Figure 5 also shows that the less evolved stars tend to have higher C abundances than more evolved ones, since they did not reach yet the first dredge-up (see Sect. 4.3).

[C/O] vs. [Fe/H] (Figure 5) shows a large dispersion. The range shown is $-0.19 \leq [\text{C}/\text{O}] \leq 0.46$, and for 6 stars [C/O] < 0 (see Table 13). Barbuy et al. (1992) found the range $0.19 \leq [\text{C}/\text{O}] \leq 0.47$. North et al. (1994) found higher values for [C/O], inside the range $0.4 \leq [\text{C}/\text{O}] \leq 1.5$.

4.3. Nitrogen

Reddy et al. (2003) derived N abundances from two N I lines for F and G dwarfs, and observed a large dispersion $-0.05 \leq [\text{N}/\text{Fe}] \leq 0.6$ at $-0.4 \leq [\text{Fe}/\text{H}] \leq 0.15$. The sample of Clegg et al. (1981) resulted in [N/Fe] ≈ 0 in the same range of metallicities.

In the present work, nitrogen abundances were determined by synthesis of CN lines in the regions $\lambda 6476 - 6480 \text{ \AA}$, $\lambda 6703 - 6709 \text{ \AA}$ and $\lambda 8030 - 8041 \text{ \AA}$, with C abundance previously established from the average of the synthesis of C_2 and CH (Sect. 4.2). Figure 8 illustrates the fits to CN bands. The CN bands are very weak in stars with higher temperatures, and for them only an upper limit was given, as indicated in Figure 5 and Table 13. The results are shown in Tables 12 and 13. [N/Fe] seems to increase toward lower metallicities, except for the star HD 123396, as shown in Figure 5. The dispersion is probably due to different degrees of mixing.

Barbuy et al. (1992) noted that the barium giants of their sample are rich in both N and C. Figure 5 and Table 13 show that the same applies to the present sample. For the star in common HD 27271, a nitrogen abundance 0.23 dex lower than

Barbuy et al. (1992) was found. Figure 5 suggests that the less evolved barium stars show larger N overabundances.

The CNO excess provides clues on the origin of the material rich in heavy elements that polluted the envelope of the barium stars, by comparing them with normal stars. During the main sequence, the H burning through CNO cycle conserves the number of nuclei of C, N and O. During the first dredge-up the atoms of ^{12}C capture protons forming ^{13}C or ^{14}N , and, as a result, the ^{12}C is depleted by ≈ 0.2 dex and the N increases by ≈ 0.3 dex. Some normal giants can reach $[\text{N}/\text{Fe}] = 0.55$ and in metal-poor stars the mixing is more efficient. The barium giants have already passed by the first dredge-up, and therefore they should carry the characteristics of this event in addition to their peculiarities. Once the O abundance is not modified and N increases for every star after the first dredge-up, the C is considered the main responsible for the CNO excess in barium stars relative to normal stars, suggesting that the origin of the material that has polluted the envelope is the He burning shell. The fact that the less evolved barium stars are rich in N suggests that N is also responsible for the CNO excess in these stars. Table 13 shows $[\sum\text{CNO}/\text{Fe}] > 0$ for all barium stars, and Figure 6 shows a clear increasing trend of $[\sum\text{CNO}/\text{Fe}]$ with T_{eff} and $\log g$. The range found by Barbuy et al. (1992) for their giants correspond to $0.06 \leq [\sum\text{CNO}/\text{Fe}] \leq 0.24$ and for the present work, $0.01 \leq [\sum\text{CNO}/\text{Fe}] \leq 0.73$, with the less evolved stars showing the higher values.

4.4. Sodium and Aluminum

It is probable that the production of Na, Mg and Al occurs through C and N burning in massive stars, and for this reason, probably the SN II are the main sources of α -, Na and Al in the disk. Sharing the same production site, the pattern of abundances are expected to show similarities, and Figure 11 shows that it is true for the program stars. For the same reason, it is interesting to study the relations involving $[\text{Al}/\text{Mg}]$ and $[\text{Na}/\text{Mg}]$ in addition to $[\text{Al}/\text{Fe}]$ and $[\text{Na}/\text{Fe}]$.

The Baumüller & Gehren (1997) analysis taking into account NLTE effects suggests that for $[\text{Fe}/\text{H}] \approx -0.5$ there is an overabundance of $[\text{Al}/\text{Fe}] \approx 0.15$ dex. According to Figure 11 and Table 14, some of the sample stars are found in this region, one of them being the halo star HD 5424 ($[\text{Fe}/\text{H}] = -0.55$). The others are below this value, except HD 210910 ($[\text{Fe}/\text{H}] = -0.37$), which is a subgiant with broad lines, and HD 123396 ($[\text{Fe}/\text{H}] = -1.19$), which is a halo giant. Most data are found in the range $-0.1 \leq [\text{Al}/\text{Fe}] \leq 0.1$. Relative to Mg, Figure 9 shows that in the range $-0.75 \leq [\text{Mg}/\text{H}] \leq 0$, 4 stars show overabundance and 19 a deficiency of Al relative to Mg, with values in the range $-0.4 \leq [\text{Al}/\text{Mg}] \leq +0.1$. In the Al abundance calculation the lines $\lambda 6696 \text{ \AA}$ and $\lambda 6698.7 \text{ \AA}$ were used.

Baumüller et al. (1998) analysed a sample of stars taking into account NLTE effects and verified a decreasing trend of Na abundance toward decreasing metallicities. The present sample stars are found to be in the range $-0.18 \leq [\text{Na}/\text{Fe}] \leq 0.31$, showing no clear trend, but most data have $-0.1 \leq [\text{Na}/\text{Fe}] \leq 0.2$, as shown in Figure 11. Relative to Mg, Figure 9 shows that the results are in the range $-0.4 \leq [\text{Na}/\text{Mg}] \leq +0.35$ with a larger

dispersion than $[\text{Al}/\text{Mg}]$. A Na deficiency relative to Mg was found in 11 stars, and for the other stars $[\text{Na}/\text{Mg}] \geq 0$. Six lines of Na I with two doublets were used. For 7 stars the difference between the lines is within ± 0.25 and ± 0.30 . For one star, the difference is 0.40 dex. For the other sample stars there is good agreement between the lines.

The Al and Na excesses relative to Ba show an increase toward higher metallicities (see Figure 16 and Table 18), while a decreasing trend is seen relative to $[\text{Ba}/\text{H}]$ (Figure 15). In the range $0 \leq [\text{Ba}/\text{H}] \leq 1.5$, $-0.2 \leq [\text{Na}/\text{Ba}] \leq -1.6$ and $-0.3 \leq [\text{Al}/\text{Ba}] \leq -1.8$ were found. Otherwise, the excesses of Al and Na relative to Eu show no trend as a function of $[\text{Fe}/\text{H}]$, with $-0.7 \leq [\text{Na}/\text{Eu}] \leq 0.2$ and $-0.8 \leq [\text{Al}/\text{Eu}] \leq 0$ (Figure 18). In the range $-0.7 \leq [\text{Eu}/\text{H}] \leq 0.4$ there is a small decreasing trend of $[\text{Al}, \text{Na}/\text{Eu}]$ toward higher $[\text{Eu}/\text{H}]$ (see Figure 17 and Table 18).

Table 15. Lines, equivalent widths and abundances. Symbols: '+' : abundances derived by using metallicities from Fe I lines; '**': multiple line; '***': Ni line blended with O line. < indicates an upper limit for oxygen. The gf-values sources are: 1 - Allende Prieto et al. (2001), 2 - Lambert (1978), 3 - NIST, 4 - Fuhrmann et al. (1995), 5 - Prochaska et al. (2000), 6 - McWilliam & Rich (1994), 7 - Barbuy et al. (1999), 8 - Bielski (1975), 9 - Biémont & Godefroid (1980), 10 - Gratton & Sneden (1994), 11 - Hannaford et al. (1982), 12 - Hannaford & Lowe (1983), 13 - Biémont et al. (1981), 14 - Thévenin (1990), 15 - Thévenin (1989), 16 - Smith et al. (2000), 17 - McWilliam (1998), 18 - Rutten (1978), 19 - Lawler et al. (2001a), 20 - Palmeri et al. (2000), 21 - Goly et al. (1991), 22 - Lage & Whaling (1976), 23 - Hartog et al. (2003), 24 - Maier & Whaling (1977), 25 - Sneden et al. (1996), 26 - Biémont et al. (1989), 27 - Lawler et al. (2001b), 28 - Bergstrom et al. (1988), 29 - Corliss & Bozman (1962), 30 - mean between Kusz (1992) and Biémont & Lowe (1993), 31 - Biémont et al. (2000) 32 - Biémont et al. (1983). Full table is only available in electronic form.

el	λ	χ_{ex}	log gf	ref	HD 749			HR 107			
					EW	log ϵ	[X/Fe]	[X/Fe]+	EW	log ϵ	[X/Fe]
O I	6300.31	0.00	-9.717	1	27	8.94	0.03	0.26	6	8.31	-0.07 ...
O I	6363.776	0.02	-10.250	2	17	8.84	-0.07	0.16
Na I	4982.808	2.10	-1.913	3	102	6.03	-0.47	-0.24	39	5.97	0.00 ...
Na I	4982.813	2.10	-0.961	3	*	6.03	-0.47	-0.24	*	5.97	0.00 ...
Na I	5682.65	2.10	-0.700	3	104	6.08	-0.42	-0.19	55	5.94	-0.03 ...
Na I	5688.193	2.104	-1.390	3	135	6.18	-0.32	-0.09	86	6.04	0.07 ...
.
.

4.5. α -elements

The observations show that the α -elements tend to be overabundant at low metallicities, with $[\text{X}/\text{Fe}]$ reaching ≈ 0.5 at $-4 < [\text{Fe}/\text{H}] < -1$ (e.g. Barbuy 1988; Cayrel et al. 2004). At $[\text{Fe}/\text{H}] \approx -1$ the overabundance starts to decrease toward higher metallicities, and $[\text{X}/\text{Fe}]$ can be subsolar at $[\text{Fe}/\text{H}] \approx 0$. This behaviour of the α -elements relative to iron has been attributed to the time delay between core-collapse supernovae and SNIa.

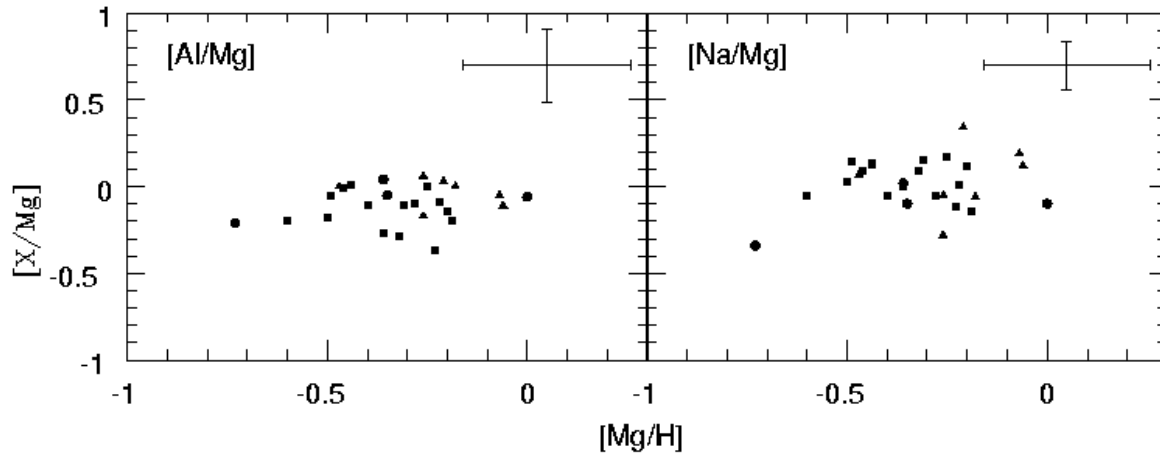


Fig. 9. $[Al/Mg]$ and $[Na/Mg]$ vs. $[Mg/H]$. Symbols are the same as in Figure 4.

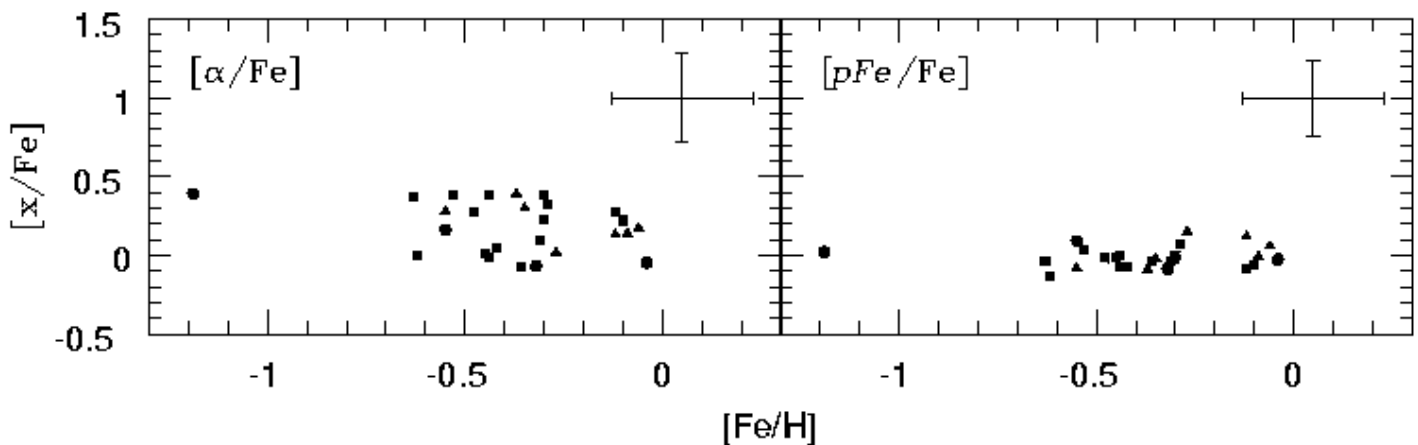


Fig. 10. $[\alpha, pFe/Fe]$ vs. $[Fe/H]$. Symbols are the same as in Figure 4.

No substantial difference between α -elements in normal and barium stars were seen up to now. Figure 10 shows $[\alpha/Fe]$ vs. $[Fe/H]$ for the sample barium stars where α 's included are O, Mg, Si, Ca and Ti.

Oxygen: It is the third most abundant element in the Universe after H and He. It is produced during He burning in the interior of massive stars, and is released through SN II events.

Abundances of oxygen for the present sample were determined through spectrum synthesis of the forbidden lines of [O I] at $\lambda 6300.3 \text{ \AA}$ and $\lambda 6363.8 \text{ \AA}$. These lines are reliable since they are not subject to NLTE effects. The resolution of the program stars spectra is such that the Sc II line at $\lambda 6300.7 \text{ \AA}$ is not blended with the [O I] line at $\lambda 6300.3 \text{ \AA}$. Telluric lines are displaced thanks to their radial velocities and do not blend the oxygen line in the sample stars. For 2 stars, HD 147609 and HD 87080, the sky emission line is present preventing the determination of the O abundance. For HD 13551, HD 22589 and HD 107574, an upper limit was derived.

The Ni I line at $\lambda 6300.335 \text{ \AA}$ was taken into account in the oxygen abundance calculations. The adopted abundance for Ni was the average of other ten lines and the atomic constants are shown in Table 15.

The solar abundance adopted was $\log \epsilon(O) = 8.74$, which is the value by Asplund et al. (2005) through a 3D atmosphere model, $\log \epsilon(O) = 8.66$, corrected by 0.08 for 1D, according to Allende Prieto et al. (2001).

The O abundance results obtained shown in Figure 11, are in good agreement with Figure 4 by François et al. (2004) in the same range of metallicities.

Magnesium: Similarly to oxygen, magnesium is also produced by massive stars, but in this case carbon and neon burning is responsible for its production. Figure 4 of François et al. (2004) shows the evolution of $[Mg/Fe]$ relative to $[Fe/H]$, where $[Mg/Fe]$ decreases toward increasing metallicities.

The 3 lines used in the determination of Mg abundance for the present sample present a good agreement, as shown in Table 15. Figure 11 shows that the range of $[Mg/Fe]$ is similar to those of $[Na/Fe]$ and $[Al/Fe]$, differing from $[Ti/Fe]$, that reaches lower abundances, in agreement with François et al. (2004, and references therein).

Silicon: SNaE of $\approx 20 M_{\odot}$ could be the main sources of Si (Woosley & Weaver 1995). Prochaska et al. (2000) found a high overabundance of Si and an increasing abundance trend toward lower metallicities for stars of the thick disk in the

Table 14. Abundance ratios of Al and Na relative to Mg, and the α and pFe relative to Fe.

star	[Al/Mg]	$\sigma_{[Al/Mg]}$	[Na/Mg]	$\sigma_{[Na/Mg]}$	[Mg/H]	$\sigma_{[Mg/H]}$	[α /Fe]	$\sigma_{[\alpha/Fe]}$	[pFe /Fe]	$\sigma_{[pFe/Fe]}$
HD 749	0.00	0.20	-0.06	0.14	-0.18	0.21	0.17	0.28	0.06	0.24
HR 107	-0.10	0.10	-0.05	0.07	-0.28	0.07	-0.08	0.11	-0.04	0.06
HD 5424	-0.05	0.20	-0.10	0.14	-0.35	0.21	0.16	0.28	0.09	0.24
HD 8270	-0.01	0.10	0.09	0.07	-0.46	0.07	0.04	0.11	-0.07	0.06
HD 12392	-0.05	0.20	0.19	0.14	-0.07	0.21	0.13	0.28	0.12	0.24
HD 13551	-0.20	0.10	-0.14	0.07	-0.19	0.07	0.38	0.11	0.00	0.06
HD 22589	-0.11	0.10	0.12	0.07	-0.06	0.07	0.02	0.11	0.15	0.06
HD 27271	0.03	0.20	0.34	0.14	-0.21	0.21	0.14	0.28	-0.01	0.24
HD 48565	-0.20	0.10	-0.05	0.07	-0.60	0.07	0.00	0.11	-0.14	0.06
HD 76225	-0.29	0.10	0.09	0.07	-0.32	0.07	0.09	0.11	-0.04	0.06
HD 87080	-0.11	0.10	-0.05	0.07	-0.40	0.07	-0.01	0.11	-0.07	0.06
HD 89948	-0.37	0.10	-0.12	0.07	-0.23	0.07	0.23	0.11	-0.03	0.06
HD 92545	-0.14	0.10	0.12	0.07	-0.20	0.07	0.27	0.11	-0.09	0.06
HD 106191	-0.09	0.10	0.01	0.07	-0.22	0.07	0.32	0.11	0.07	0.06
HD 107574	0.00	0.10	0.07	0.07	-0.47	0.07	0.28	0.11	-0.08	0.06
HD 116869	0.04	0.20	0.02	0.14	-0.36	0.21	-0.07	0.28	-0.09	0.24
HD 123396	-0.21	0.20	-0.34	0.14	-0.73	0.21	0.39	0.28	0.02	0.24
HD 123585	0.01	0.10	0.13	0.07	-0.44	0.07	0.27	0.11	-0.02	0.06
HD 147609	-0.05	0.10	0.14	0.07	-0.49	0.07	0.01	0.11	-0.02	0.06
HD 150862	0.00	0.10	0.17	0.07	-0.25	0.07	0.22	0.11	-0.06	0.06
HD 188985	-0.11	0.10	0.15	0.07	-0.31	0.07	0.38	0.11	0.00	0.06
HD 210709	-0.06	0.20	-0.10	0.14	0.00	0.21	-0.05	0.28	-0.03	0.24
HD 210910	0.06	0.20	-0.28	0.14	-0.26	0.21	0.39	0.28	-0.09	0.24
HD 222349	-0.18	0.10	0.03	0.07	-0.50	0.07	0.37	0.11	-0.04	0.06
BD+18 5215	-0.27	0.10	0.00	0.07	-0.36	0.07	0.38	0.11	0.03	0.06
HD 223938	-0.17	0.20	-0.05	0.14	-0.26	0.21	0.30	0.28	-0.02	0.24

range of metallicities $-1.2 < [Fe/H] < -0.3$, in agreement with McWilliam (1997).

For the present sample 5 lines were used. All lines give similar abundances, except the line $\lambda 5948.5 \text{ \AA}$ that gives values 0.5 dex higher for some stars, possibly due to an unknown blend. Most results give $[Si/Fe] \approx 0$, except for the star HD 123396, a halo giant, for which the abundance is higher, as shown in Figure 11. The results are in agreement with the chemical evolution model by François et al. (2004) for this range of metallicities. The odd-even effect observed by Arnett (1971), where Mg and Si are overabundant relative to Na and Al, is confirmed for some sample stars. For several stars, Na and Al abundances are higher than Si and Mg, with $-0.1 \leq [Mg/Fe] \leq 0.2$, $-0.15 \leq [Si/Fe] \leq 0.2$, $-0.1 \leq [Na/Fe] \leq 0.2$ and $-0.1 \leq [Al/Fe] \leq 0.1$.

Calcium: According to McWilliam (1997), the abundance of Ca is expected to behave similarly to Si, given that SN II of moderate mass is the main source of both elements (Woosley & Weaver 1995), and they can be also released by SN Ia (Nomoto et al. 1997b). The similarity of behaviour between Ca and Si was verified by Prochaska et al. (2000) as well as for the barium stars of the present sample (Figure 11), except for the star HD 210910. Six Ca lines were used, being some of them very strong in some sample stars (Table 15). For 16 stars the difference between abundances derived from those lines is from 0.2 to 0.5 dex, and for the others, there is a better agreement.

Titanium: Ti is usually included in the α -elements list because its overabundance in metal-poor stars is similar to that of α -elements (Gratton & Sneden 1991), but its nucleosynthesis is unclear (Woosley & Weaver 1995). For this reason, Ti abundance can be different from that of Ca and Si, as observed by Prochaska et al. (2000). According to François et al. (2004), Ti and Mg abundances have a similar behaviour, though the dispersion is larger for Mg in their Figure 4.

In the present work, Ti abundances are usually lower than those of Ca, Si and Mg, as shown in Figures 11 and 12. Twelve lines of Ti I were used. For 4 stars, the abundance from the $\lambda 5210.4 \text{ \AA}$ line is different from the other lines. The reason for that difference is unclear. If the problem were in the atomic constants, the difference would be observed for all stars. In general, the abundance results from the 12 lines are in agreement.

4.6. Iron peak elements

At the last moments of the life of a massive star, the iron and the iron peak elements are formed in large amounts (Woosley & Weaver 1995). The process that precedes the explosion of SN Ia also produces these elements, but in lower amounts relative to massive stars. However, the SN Ia ejecta contain larger amounts of those elements than SN II, because part of the yield is restrained in the neutron star newly formed.

Figure 12 of McWilliam (1997) shows abundances from previous work, and it is possible to observe the trends of $[X/Fe]$

Table 16. Mean $\log \epsilon(X)$ and $[X/Fe]$. The symbol “*” indicates that the metallicity was derived from Fe I lines.

el	HD 749			HR 107		HD 5424		HD 8270		HD 12392		HD 13551			HD 22589	
	$\log \epsilon(X)$	$[X/Fe]$	$[X/Fe]^*$	$\log \epsilon(X)$	$[X/Fe]$	$\log \epsilon(X)$	$[X/Fe]$	$\log \epsilon(X)$	$[X/Fe]$	$\log \epsilon(X)$	$[X/Fe]$	$\log \epsilon(X)$	$[X/Fe]$	$[X/Fe]^*$	$\log \epsilon(X)$	$[X/Fe]$
O	8.89	-0.02	0.21	8.31	-0.07	8.37	0.18	8.40	0.08	8.80	0.18	<8.73	<0.23	<0.43	<8.50	<0.03
Na	6.09	-0.41	-0.18	6.00	0.03	5.88	0.10	5.96	0.05	6.45	0.24	6.00	-0.09	0.11	6.39	0.33
Mg	7.40	-0.35	-0.12	7.30	0.08	7.23	0.20	7.12	-0.04	7.51	0.05	7.39	0.05	0.25	7.52	0.21
Al	6.29	-0.35	-0.12	6.09	-0.02	6.07	0.15	6.00	-0.05	6.35	0.00	6.08	-0.15	0.05	6.30	0.10
Si	7.66	-0.06	0.17	7.13	-0.06	7.20	0.20	7.11	-0.02	7.34	-0.09	7.21	-0.10	0.10	7.32	0.04
Ca	6.28	-0.25	-0.02	6.04	0.04	5.71	-0.10	6.01	0.07	6.23	-0.01	6.12	0.00	0.20	6.44	0.35
Sc	3.42	0.08	0.31	3.00	0.19	3.11	0.49	3.01	0.26	3.48	0.43	2.98	0.05	0.25	3.06	0.16
Ti	4.75	-0.44	-0.21	4.69	0.03	4.41	-0.06	4.47	-0.13	5.03	0.13	4.53	-0.25	-0.05	4.77	0.02
V	3.93	-0.24	-0.01	3.70	0.06	3.28	-0.17	3.36	-0.22	3.94	0.06	3.58	-0.18	0.02	3.65	-0.08
Cr	5.51	-0.33	-0.10	5.28	-0.03	5.14	0.02	5.13	-0.12	5.64	0.09	5.17	-0.26	-0.06	5.63	0.23
Co	5.37	0.28	0.51	4.74	0.18	4.66	0.29	4.43	-0.07	5.27	0.47	4.48	-0.20	0.00	4.73	0.08
Ni	6.25	-0.17	0.06	5.83	-0.06	5.79	0.09	5.77	-0.06	6.23	0.10	5.82	-0.19	0.01	6.11	0.13
Cu	4.20	-0.18	0.05	3.68	-0.17	3.49	-0.17	3.58	-0.21	4.18	0.09	3.60	-0.37	-0.17	3.94	0.00
Zn	4.53	-0.24	-0.01	4.14	-0.10	4.15	0.10	4.14	-0.04	4.50	0.02	4.26	-0.10	0.10	4.44	0.11
Sr I	3.49	0.35	0.58	2.91	0.30	3.37	0.95	3.38	0.83	3.90	1.05	3.29	0.56	0.76	3.53	0.83
Sr II	3.59	0.45	0.68	3.36	0.75	3.02	0.60	3.45	0.90	3.63	0.78	3.53	0.80	1.00	3.58	0.88
Y	3.36	0.95	1.18	2.48	0.60	2.72	1.03	2.77	0.95	3.33	1.21	2.88	0.88	1.08	2.80	0.83
Zr I	2.86	0.09	0.32	2.84	0.60	2.54	0.49	3.02	0.84	3.20	0.72	3.05	0.69	0.89	2.82	0.49
Zr II	3.99	1.22	1.45	2.81	0.57	3.40	1.35	3.18	1.00	3.84	1.36	3.18	0.82	1.02	3.40	1.07
Mo	1.99	-0.10	0.13	2.16	0.60	1.57	0.20	2.10	0.60	2.30	0.50	2.28	0.60	0.80	1.85	0.20
Ba	3.25	0.95	1.18	2.72	0.95	3.06	1.48	2.82	1.11	3.52	1.51	2.85	0.96	1.16	2.74	0.88
La	2.33	1.03	1.26	1.44	0.67	2.13	1.55	1.71	1.00	2.62	1.61	1.68	0.79	0.99	1.56	0.70
Ce	3.14	1.27	1.50	1.75	0.41	3.01	1.86	2.11	0.83	3.25	1.67	2.17	0.71	0.91	1.88	0.45
Pr	1.49	0.66	0.89	0.82	0.52	1.49	1.38	0.72	0.48	1.93	1.39	0.79	0.37	0.57	0.66	0.27
Nd	2.72	1.10	1.33	1.41	0.32	2.62	1.72	1.76	0.73	2.82	1.49	1.74	0.53	0.73	1.50	0.32
Sm	1.88	0.70	0.93	0.95	0.30	1.73	1.27	0.96	0.37	2.36	1.47	1.02	0.25	0.45	0.82	0.08
Eu	0.79	0.10	0.33	0.20	0.04	0.43	0.46	0.42	0.32	0.88	0.48	0.29	0.01	0.21	0.46	0.21
Gd	1.38	0.09	0.32	1.31	0.55	1.02	0.45	0.95	0.25	1.57	0.57	1.23	0.35	0.55	0.88	0.03
Dy	2.06	0.69	0.92	2.30	1.65	0.82	0.04	1.83	0.75	0.85	-0.11	0.09	0.97	0.04
Pb	2.27	0.15	0.38	2.49	0.90	2.50	1.10	2.03	0.50	2.98	1.15	2.01	0.30	0.50	1.53	-0.15

el	HD 27271			HD 48565		HD 76225		HD 87080		HD 89948		HD 92545		HD 106191	
	$\log \epsilon(X)$	$[X/Fe]$	$[X/Fe]^*$	$\log \epsilon(X)$	$[X/Fe]$	$\log \epsilon(X)$	$[X/Fe]$	$\log \epsilon(X)$	$[X/Fe]$	$\log \epsilon(X)$	$[X/Fe]$	$\log \epsilon(X)$	$[X/Fe]$	$\log \epsilon(X)$	$[X/Fe]$
O	8.84	-0.07	0.19	8.15	0.03	8.56	0.13	8.72	0.28	8.95	0.33	8.83	0.38
Na	6.46	-0.04	0.22	5.68	-0.03	6.10	0.08	5.88	-0.01	5.98	-0.05	6.25	0.04	6.12	0.08
Mg	7.37	-0.38	-0.12	6.98	0.02	7.26	-0.01	7.18	0.04	7.35	0.07	7.38	-0.08	7.36	0.07
Al	6.29	-0.35	-0.09	5.67	-0.18	5.86	-0.30	5.96	-0.07	5.87	-0.30	6.13	-0.22	6.16	-0.02
Si	7.45	-0.27	-0.01	6.87	-0.06	7.21	-0.03	7.02	-0.09	7.19	-0.06	7.29	-0.14	7.18	-0.08
Ca	6.20	-0.33	-0.07	5.79	0.05	6.16	0.11	6.04	0.12	6.10	0.04	6.32	0.08	6.17	0.10
Sc	3.42	0.08	0.34	2.82	0.27	3.09	0.23	3.13	0.40	2.95	0.08	3.23	0.18	3.03	0.15
Ti	4.69	-0.50	-0.24	4.35	-0.05	4.59	-0.12	4.53	-0.05	4.56	-0.16	4.78	-0.12	4.70	-0.03
V	3.63	-0.54	-0.28	3.19	-0.19	3.46	-0.23	3.42	-0.14	3.60	-0.10	3.77	-0.11	3.77	0.06
Cr	5.35	-0.49	-0.23	4.88	-0.17	5.24	-0.12	5.13	-0.10	5.37	0.00	5.42	-0.13	5.45	0.07
Co	5.00	-0.09	0.17	4.22	-0.08	4.64	0.03	4.48	0.00	4.60	-0.02	4.82	0.02	4.78	0.15
Ni	6.19	-0.23	0.03	5.50	-0.13	5.91	-0.03	5.74	-0.07	5.91	-0.04	6.04	-0.09	6.03	0.07
Cu	4.01	-0.37	-0.11	3.27	-0.32	3.78	-0.12	3.52	-0.25	3.74	-0.17	3.82	-0.27	3.88	-0.04
Zn	4.47	-0.30	-0.04	4.01	0.03	4.27	-0.02	4.26	0.10	4.32	0.02	4.33	-0.15	4.39	0.08
Sr I	3.37	0.23	0.49	3.32	0.97	3.74	1.08	3.51	0.98	3.65	0.98	3.52	0.67	3.63	0.95
Sr II	3.52	0.38	0.64	3.39	1.04	3.92	1.26	3.53	1.00	3.75	1.08	3.58	0.73	3.33	0.65
Y	3.04	0.63	0.89	2.63	1.01	3.10	1.17	2.91	1.11	2.96	1.02	2.76	0.64	2.86	0.91
Zr I	2.65	-0.12	0.14	2.71	0.73	3.47	1.18	2.96	0.80	3.15	0.85	3.03	0.55
Zr II	3.55	0.78	1.04	3.17	1.19	3.55	1.26	3.51	1.35	3.33	1.03	3.23	0.75	3.38	1.07
Mo	1.79	-0.30	-0.04	1.80	0.50	2.21	0.60	1.88	0.40	2.12	0.50	2.20	0.40	2.13	0.50
Ba	2.92	0.62	0.88	2.80	1.29	3.17	1.35	3.17	1.48	2.82	0.99	3.05	1.04	2.72	0.88
La	1.76	0.46	0.72	1.90	1.39	2.04	1.22	2.43	1.74	1.76	0.93	1.73	0.72	1.50	0.66
Ce	2.27	0.40	0.66	2.68	1.60	2.45	1.06	2.99	1.73	2.11	0.71	2.18	0.60	2.02	0.61
Pr	1.06	0.23	0.49	1.13	1.09	1.10	0.75	1.46	1.24	0.96	0.60	0.98	0.44	1.21	0.84
Nd	1.89	0.27	0.53	2.14	1.31	1.91	0.77	2.57	1.56	1.80	0.65	1.75	0.42	1.64	0.48
Sm	1.33	0.15	0.41	1.34	0.95	1.23	0.53	1.69	1.12	1.14	0.43	1.13	0.24	1.18	0.46
Eu	0.74	0.05	0.31	0.25	0.35	0.46	0.25	0.74	0.66	0.38	0.16	0.72	0.32	0.43	0.20
Gd	1.28	-0.01	0.25	1.19	0.69	1.25	0.44	1.58	0.90	1.07	0.25	1.14	0.14	1.23	0.40
Dy	1.31	-0.06	0.20	1.27	0.69	1.18	0.29	1.90	1.14	0.59	-0.31	1.17	0.09	1.20	0.29
Pb	2.17	0.05	0.31	2.68	1.35	2.49	0.85	2.56	1.05	2.00	0.35	2.53	0.70	2.31	0.65

The usual notations were adopted: $\log \epsilon(A) = \log(N_A/N_H)+12$ and $[A/B] = \log(N_A/N_B)_* - \log(N_A/N_B)_\odot$, where N_A and N_B are the numerical particle density of “A” and “B”, respectively.

relative to metallicity for iron peak elements. In the present work, this trend is unclear. However, in average, $[pFe/Fe] \approx 0$ at $-1.2 < [Fe/H] < 0$, as shown in Figure 10, being pFe the average of V, Cr, Co and Ni abundances.

The stellar yield of iron peak elements is uncertain given that it depends on several process not well established such as the amount of mass released during supernovae events, the mass retained in the proto neutron star, the energy of the explosion and the neutron flux.

Table 17. Same as Table 16 for other 12 sample stars and $\log \epsilon(X)$ for the Sun. For solar abundances the errors on last decimals are given in parenthesis.

el	HD 107574		HD 116869		HD 123396			HD 123585		HD 147609			HD 150862		HD 188985	
	$\log \epsilon(X)$	[X/Fe]	$\log \epsilon(X)$	[X/Fe]	$\log \epsilon(X)$	[X/Fe]	[X/Fe]*	$\log \epsilon(X)$	[X/Fe]	$\log \epsilon(X)$	[X/Fe]	[X/Fe]*	$\log \epsilon(X)$	[X/Fe]	$\log \epsilon(X)$	[X/Fe]
O	<8.52	<0.33	8.38	-0.04	7.97	0.22	0.42	8.59	0.33	8.92	0.28	8.88	0.44
Na	5.93	0.15	5.99	-0.02	5.26	-0.08	0.12	6.02	0.17	5.98	-0.43	0.10	6.25	0.02	6.17	0.14
Mg	7.11	0.08	7.22	-0.04	6.85	0.26	0.46	7.14	0.04	7.09	-0.57	-0.04	7.33	-0.15	7.27	-0.01
Al	6.00	0.08	6.15	0.00	5.53	0.05	0.25	6.04	0.05	5.93	-0.62	-0.09	6.22	-0.15	6.05	-0.12
Si	7.01	0.01	7.21	-0.02	6.65	0.09	0.29	7.01	-0.06	7.16	-0.47	0.06	7.32	-0.13	7.19	-0.06
Ca	5.88	0.07	5.88	-0.16	5.25	-0.12	0.08	5.95	0.07	5.88	-0.56	-0.03	6.21	-0.05	6.14	0.08
Sc	2.70	0.08	2.98	0.13	2.45	0.27	0.47	2.89	0.20	3.43	0.18	0.71	3.32	0.25	3.11	0.24
Ti	4.43	-0.04	4.54	-0.16	3.76	-0.27	-0.07	4.59	0.05	4.41	-0.69	-0.16	4.86	-0.06	4.70	-0.02
V	3.56	0.11	3.41	-0.27	2.48	-0.53	-0.33	3.63	0.11	3.35	-0.73	-0.20	3.78	-0.12	3.75	0.05
Cr	4.97	-0.15	5.12	-0.23	4.25	-0.43	-0.23	5.12	-0.07	5.12	-0.63	-0.10	5.50	-0.07	5.41	0.04
Co	4.44	0.07	4.73	0.13	3.90	-0.03	0.17	4.78	0.34	4.46	-0.54	-0.01	4.90	0.08	4.68	0.06
Ni	5.63	-0.07	5.86	-0.07	5.12	-0.14	0.06	5.74	-0.03	5.80	-0.53	0.00	6.09	-0.06	5.93	-0.02
Cu	3.44	-0.22	3.65	-0.24	2.83	-0.39	-0.19	3.77	0.04	3.66	-0.63	-0.10	3.99	-0.12	3.80	-0.11
Zn	4.01	-0.04	4.25	-0.03	3.84	0.23	0.43	4.22	0.10	4.29	-0.39	0.14	4.50	0.00	4.37	0.07
Sr I	3.02	0.60	3.08	0.43	2.40	0.42	0.62	3.59	1.10	3.56	0.51	1.04	3.68	0.81	3.72	1.05
Sr II	3.52	1.10	2.90	0.25	2.18	0.20	0.40	3.70	1.21	4.11	1.06	1.59	3.57	0.70	3.65	0.98
Y	2.65	0.96	2.51	0.59	1.75	0.50	0.70	3.10	1.34	3.36	1.04	1.57	3.22	1.08	2.96	1.02
Zr I	2.31	0.03	1.31	-0.30	-0.10	3.57	1.45	3.04	0.36	0.89	3.51	1.01	2.95	0.65
Zr II	3.00	0.95	2.96	0.68	2.60	0.99	1.19	3.48	1.36	3.71	1.03	1.56	3.62	1.12	3.48	1.18
Mo	2.27	0.90	1.40	-0.20	0.53	-0.40	-0.20	2.44	1.00	2.20	0.20	0.73	2.32	0.50	2.12	0.50
Ba	3.29	1.71	2.83	1.02	2.24	1.10	1.30	3.44	1.79	3.25	1.04	1.57	3.06	1.03	3.03	1.20
La	1.74	1.16	1.77	0.96	1.21	1.07	1.27	2.30	1.65	2.31	1.10	1.63	1.83	0.80	1.99	1.16
Ce	2.17	1.02	2.28	0.90	2.13	1.42	1.62	2.91	1.69	2.89	1.11	1.64	2.15	0.55	2.63	1.23
Pr	0.81	0.70	0.98	0.64	0.67	1.00	1.20	1.49	1.31	1.43	0.69	1.22	1.01	0.45	1.18	0.82
Nd	1.76	0.86	1.99	0.86	1.81	1.35	1.55	2.38	1.41	2.32	0.79	1.32	1.69	0.34	2.19	1.04
Sm	1.10	0.64	1.25	0.56	1.01	0.99	1.19	1.73	1.20	1.65	0.56	1.09	1.14	0.23	1.43	0.72
Eu	0.44	0.47	0.36	0.16	-0.17	0.30	0.50	0.87	0.83	0.81	0.21	0.74	0.62	0.20	0.51	0.29
Gd	0.93	0.36	1.02	0.22	0.74	0.61	0.81	1.19	0.55	1.47	0.27	0.80	1.25	0.23	1.36	0.54
Dy	0.99	0.34	1.43	0.55	1.20	0.99	1.19	1.36	0.64	1.45	0.17	0.70	1.24	0.14	1.09	0.19
Pb	2.45	1.05	2.48	0.85	1.96	1.00	1.20	3.02	1.55	2.28	0.25	0.78	2.55	0.70	2.60	0.95

el	HD 210709		HD 210910			HD 222349		BD+18 5215		HD 223938			Sun	
	$\log \epsilon(X)$	[X/Fe]	$\log \epsilon(X)$	[X/Fe]	[X/Fe]*	$\log \epsilon(X)$	[X/Fe]	$\log \epsilon(X)$	[X/Fe]	$\log \epsilon(X)$	[X/Fe]	[X/Fe]*	$\log \epsilon(X)$	ref
O	8.68	-0.02	8.81	0.03	0.44	8.54	0.43	8.64	0.43	8.74	0.13	0.35	8.74(6)	1
Na	6.23	-0.06	5.79	-0.58	-0.17	5.86	0.16	5.97	0.17	6.02	-0.18	0.04	6.33(3)	2
Mg	7.58	0.04	7.32	-0.30	0.11	7.08	0.13	7.22	0.17	7.32	-0.13	0.09	7.58(5)	2
Al	6.41	-0.02	6.27	-0.24	0.17	5.79	-0.05	5.84	-0.10	6.04	-0.30	-0.08	6.47(7)	2
Si	7.39	-0.12	7.35	-0.24	0.17	6.89	-0.03	7.07	0.05	7.23	-0.19	0.03	7.55(5)	2
Ca	6.11	-0.21	5.54	-0.86	-0.45	5.82	0.09	5.90	0.07	6.07	-0.16	0.06	6.36(2)	2
Sc	3.31	0.18	3.08	-0.13	0.28	2.76	0.22	2.82	0.18	3.14	0.10	0.32	3.17(10)	2
Ti	4.73	-0.25	4.14	-0.92	-0.51	4.34	-0.05	4.45	-0.04	4.51	-0.38	-0.16	5.02(6)	2
V	3.92	-0.04	3.35	-0.69	-0.28	3.51	0.14	3.56	0.09	3.46	-0.41	-0.19	4.00(2)	2
Cr	5.60	-0.03	4.62	-1.09	-0.68	4.90	-0.14	5.14	0.00	5.14	-0.40	-0.18	5.67(3)	2
Co	5.21	0.33	4.69	-0.27	0.14	4.26	-0.03	4.74	0.35	4.70	-0.09	0.13	4.92(4)	2
Ni	6.15	-0.06	5.86	-0.43	-0.02	5.60	-0.02	5.74	0.02	5.91	-0.21	0.01	6.25(4)	2
Cu	4.00	-0.17	3.68	-0.57	-0.16	3.39	-0.19	3.59	-0.09	3.71	-0.37	-0.15	4.21(4)	2
Zn	4.40	-0.16	4.41	-0.23	0.18	4.01	0.04	4.12	0.05	4.32	-0.15	0.07	4.60(8)	2
Sr I	3.26	0.33	3.06	0.05	0.46	3.24	0.90	3.55	1.11	3.21	0.37	0.59	2.97(7)	2
Sr II	3.02	0.09	3.46	0.45	0.86	3.39	1.05	3.59	1.15	3.23	0.39	0.61	2.97(7)	2
Y	2.73	0.53	2.41	0.13	0.54	2.64	1.03	2.72	1.01	2.63	0.52	0.74	2.24(3)	2
Zr I	2.47	-0.09	2.12	-0.52	-0.11	3.20	1.23	3.37	1.30	2.41	-0.06	0.16	2.60(2)	2
Zr II	3.35	0.79	2.59	-0.05	0.36	3.19	1.22	3.32	1.25	3.31	0.84	1.06	2.60(2)	2
Mo	1.58	-0.30	1.36	-0.60	-0.19	1.79	0.50	2.09	0.70	1.49	-0.30	-0.08	1.92(5)	2
Ba	2.82	0.73	2.75	0.58	0.99	2.88	1.38	3.06	1.46	3.00	1.00	1.22	2.13(5)	2
La	1.77	0.68	1.50	0.33	0.74	1.85	1.35	1.79	1.19	1.82	0.82	1.04	1.13(3)	3
Ce	2.40	0.74	1.98	0.24	0.65	2.47	1.40	2.28	1.11	2.39	0.82	1.04	1.70(4)	4
Pr	1.01	0.39	1.15	0.45	0.86	0.92	0.89	1.01	0.88	0.88	0.35	0.57	0.66(15)	5
Nd	2.04	0.63	1.63	0.14	0.55	2.08	1.26	1.75	0.83	2.18	0.86	1.08	1.45(1)	6
Sm	1.27	0.30	1.05	0.00	0.41	1.26	0.88	1.18	0.70	1.41	0.53	0.75	1.01(6)	7
Eu	0.56	0.08	0.69	0.13	0.54	0.13	0.24	0.23	0.24	0.54	0.15	0.37	0.52(1)	8
Gd	1.03	-0.05	1.31	0.15	0.56	1.06	0.57	1.74	1.15	1.14	0.15	0.37	1.12(4)	2
Dy	1.31	0.15	1.13	-0.11	0.30	1.16	0.59	1.21	0.54	1.36	0.29	0.51	1.20(6)	9
Pb	2.36	0.45	1.54	-0.45	-0.04	2.77	1.45	1.87	0.45	2.57	0.75	0.97	1.95(8)	2

References on solar abundances: 1 - Asplund et al. (2005); 2 - Grevesse & Sauval (1998); 3 - Lawler et al. (2001a); 4 - Palmeri et al. (2000); 5 - Lage & Whaling (1976); 6 - Hartog et al. (2003); 7 - Bi emont et al. (1989); 8 - Lawler et al. (2001b); 9 - Bi emont & Lowe (1993)

Scandium: Zhao & Magain (1990) have found Sc overabundances of ≈ 0.25 dex in metal-poor stars. Gratton & Sneden (1991) suggested that such result was

a consequence of gf-values adopted. Prochaska et al. (2000) found Sc overabundance ≈ 0.20 dex at $[Fe/H] \sim -0.5$, with a decreasing trend for lower metallicities, using $\log gf$ from

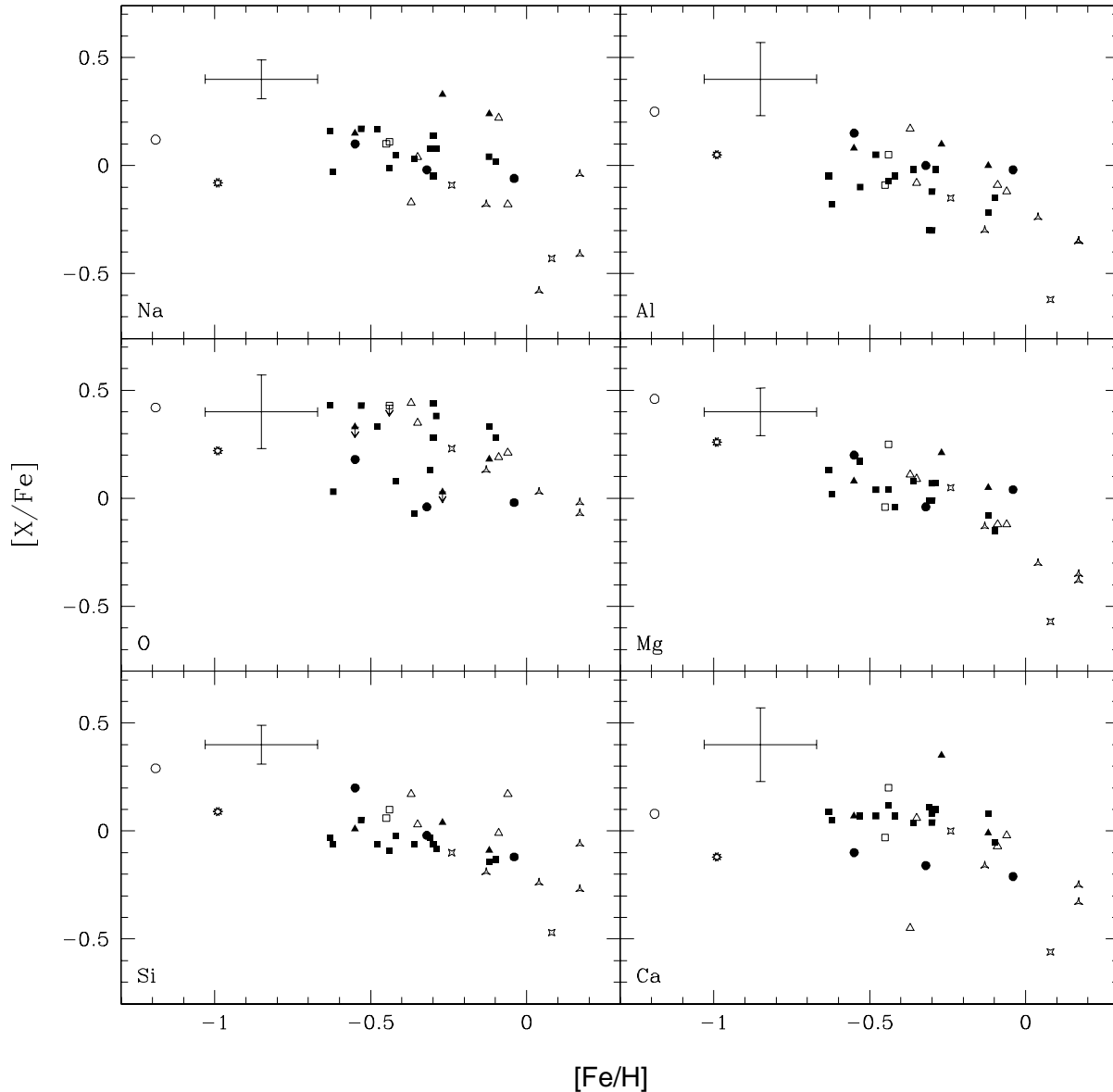


Fig. 11. $[X/Fe]$ vs. $[Fe/H]$. The symbols carry a double information: luminosity class and $\Delta[Fe/H]=[FeI/H]-[FeII/H]$. 4-pointed symbols (squares and stars): dwarf stars with $\log g \geq 3.7$; 3-pointed symbols (triangles and stars): subgiants stars with $2.4 < \log g < 3.7$; round symbols (circles and star): giants stars with $\log g \leq 2.4$. Filled symbols indicate $\Delta[Fe/H] < 0.2$ dex, being the adopted metallicities derived from Fe II lines. Open symbols indicate the seven stars for which $\Delta[Fe/H] > 0.2$ dex. These stars are represented twice being circles, triangles and squares corresponding to metallicities derived from Fe I lines and starred symbols, the same stars with metallicities derived from Fe II lines. The arrows in the oxygen panel indicate an upper limit for HD 13551, HD 22589 and HD 107574.

Martin et al. (1988) and Lawler & Dakin (1989) for disk stars in the range $-1.2 \leq [Fe/H] \leq -0.3$. Nissen et al. (2000) found a trend of $[Sc/Fe]$ similar that of α -elements for 100 dwarf F and G stars with $-1.4 < [Fe/H] < 0$, by using hyperfine structure from Steffen (1985). In the chemical evolution model of Sc by François et al. (2004), $[Sc/Fe] \approx 0.2$ for very metal-poor stars, with a trend toward zero for stars richer than $[Fe/H] \sim -2$.

In the present work, 4 lines of Sc were used, with good agreement among their abundance results. The gf-values adopted were those from NIST. All results for $[Sc/Fe]$ shown in Figure 12 are above solar, reaching 0.7 for the star HD 147609 ($[Fe I/H]=-0.45$).

Vanadium: Few studies on vanadium were found. Gratton & Sneden (1991) analysed a sample of 20 stars in an extensive range of metallicities and found $[V/Fe] \sim 0$ for all

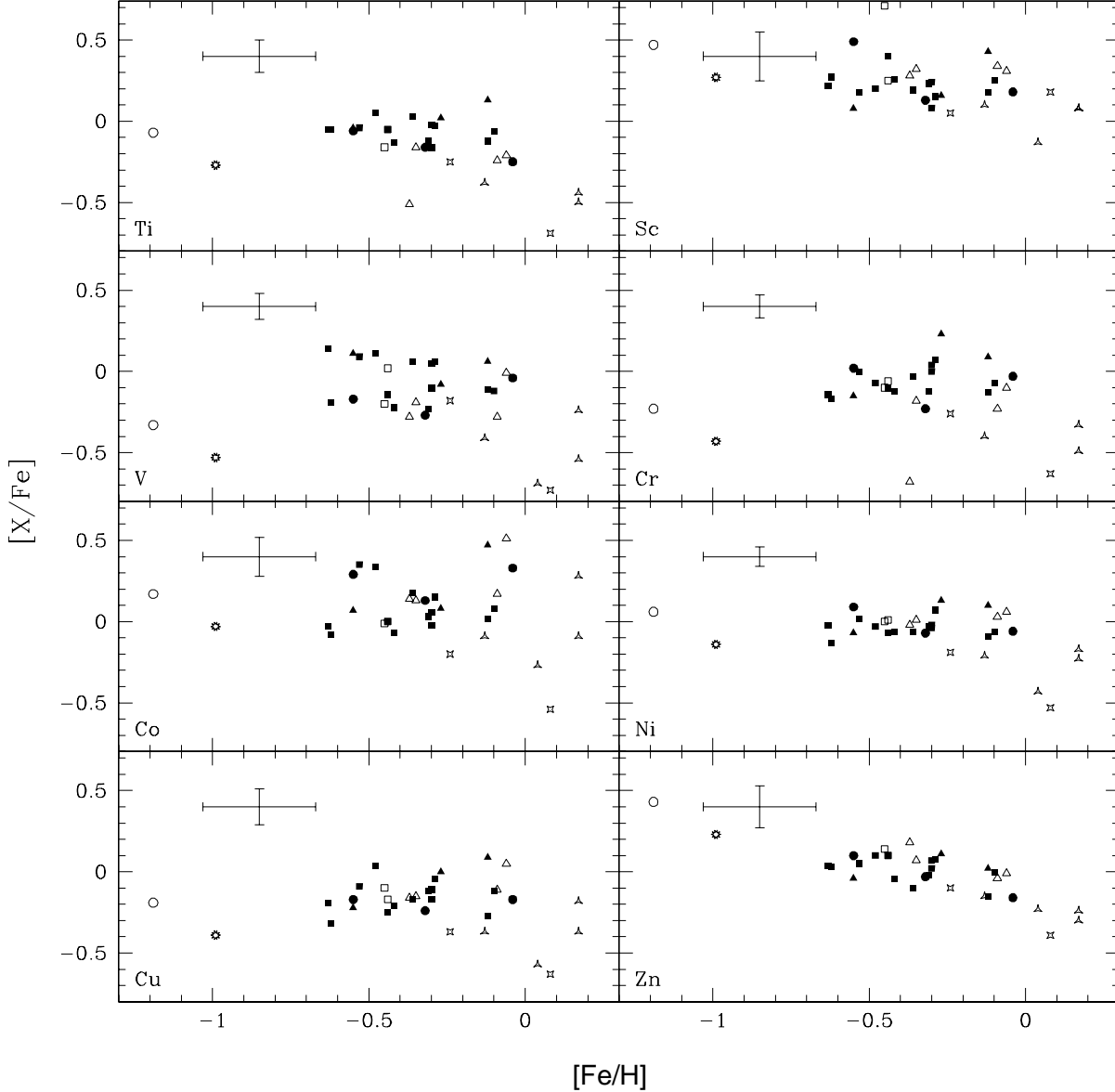


Fig. 12. $[X/Fe]$ vs. $[Fe/H]$. Symbols are the same as in Figure 11.

metallicities, in agreement with the work by Pagel (1968). However, Prochaska et al. (2000) obtained $0.1 < [V/Fe] < 0.4$.

The V I lines are very sensitive to temperature. They are usually weak for all stars of the present sample, but they are weaker for hotter stars. As an example, only 2 lines are available for the stars HD 123585 and BD+18 5215. Despite the strength of the lines, the abundances derived show a good agreement. A larger difference, of 0.5 dex was obtained for 2 lines of the star HD 210910 (see Table 15). All abundances are in the range $-0.40 < [V/Fe] < 0.2$, as shown in Figure 12.

Chromium: Cayrel et al. (2004) found an increasing trend of $[Cr/Fe]$ in the range $-4 \leq [Cr/Fe] \leq -2$ for very metal-poor stars. Figure 6 from François et al. (2004) shows that for higher metallicities, the data remain around $[Cr/Fe] \sim 0$. In the present

work, 6 lines of Cr were used, resulting in the range $-0.2 \leq [Cr/Fe] \leq 0.2$, consistent with François et al. (2004). For the star HD 210910 the result is lower than for other stars.

Cobalt: In the same range of metallicity, Prochaska et al. (2000) found an overabundance of Co relative to Fe reaching ~ 0.2 dex, whereas Gratton & Sneden (1991) found a deficiency of 0.1 dex. The lines of Co are sensitive to temperature. For the hotter stars of the sample, the equivalent widths are very small and in some cases, they had to be discarded. Differences in the abundances from different lines are shown in Table 15, and Figure 12 shows that $-0.15 < [Co/Fe] < 0.4$.

Nickel: Gratton & Sneden (1991), Edvardsson et al. (1993), Peterson et al. (1990), McWilliam et al. (1995) and Ryan et al. (1996) find $-0.1 \leq [Ni/Fe] \leq 0.1$ in the range $-4 \leq [Fe/H] \leq$

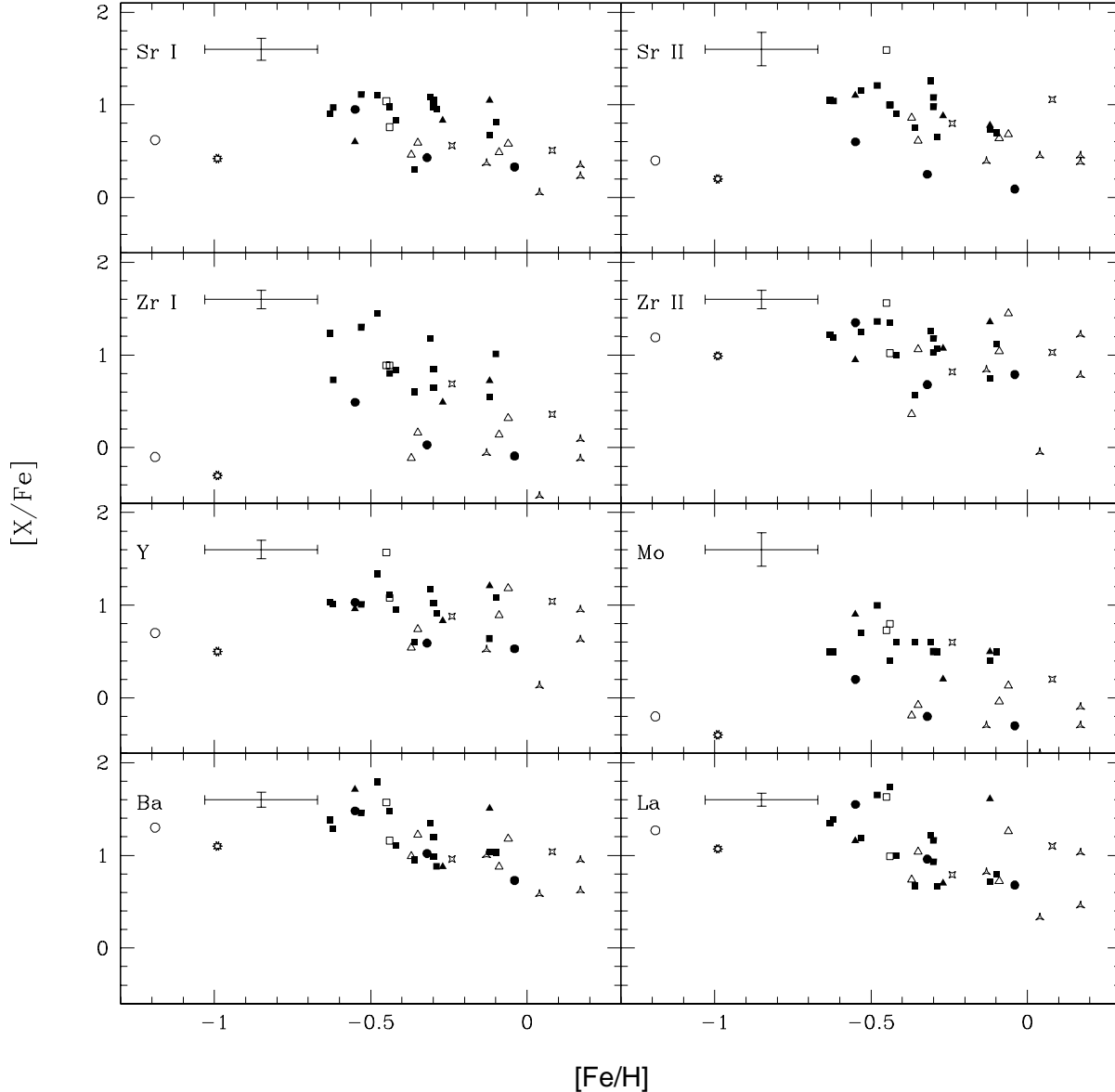


Fig. 13. $[X/Fe]$ vs. $[Fe/H]$ for heavy elements. Symbols are the same as in Figure 11.

0. In the present work, 10 lines of Ni were used with small differences between them. Figure 12 shows that $-0.13 \leq [Ni/Fe] \leq 0.12$, in agreement with François et al. (2004).

Copper: The analysis of Cu as a function of metallicity by Sneden & Crocker (1988) and Sneden et al. (1991) showed a linear decrease of $[Cu/Fe]$ toward decreasing metallicities, reaching $[Cu/Fe] \sim -1$ at $[Fe/H] \sim -3$. This trend was confirmed by Mishenina et al. (2002), who extended the sample for halo field giants, and by Simmerer et al. (2003), whose sample included 117 giant stars in 10 globular clusters in the range of metallicities $-2.4 \leq [Fe/H] \leq -0.8$.

The nucleosynthetic sites of Cu are not well established yet. Sneden et al. (1991) suggested that the Cu nucleosynthesis occurs mainly through the weak component of the s-process and

a small contribution of the explosive burning in SN II. The additional source of Cu could be SN Ia or SN II (Matteucci et al. 1993; Timmes et al. 1995; Baraffe & Takahashi 1993).

In the present work, 3 lines of Cu were used taking into account the hyperfine structure. For some stars, abundance results derived from the line $\lambda 5218.2 \text{ \AA}$ are higher than those from the other 2 lines, $\lambda 5105.5 \text{ \AA}$ and $\lambda 5782.1 \text{ \AA}$. It could be due to the gf-value, taken from a different source. However, for only one star the abundance difference between $\lambda 5218.2 \text{ \AA}$ and the other lines reaches 0.4 dex and for 3 stars, this difference is 0.25 to 0.3 dex. For the other stars, the agreement among the abundance results derived from those lines is very satisfactory. Except for a few stars, $[Cu/Fe]$ is below solar for all stars

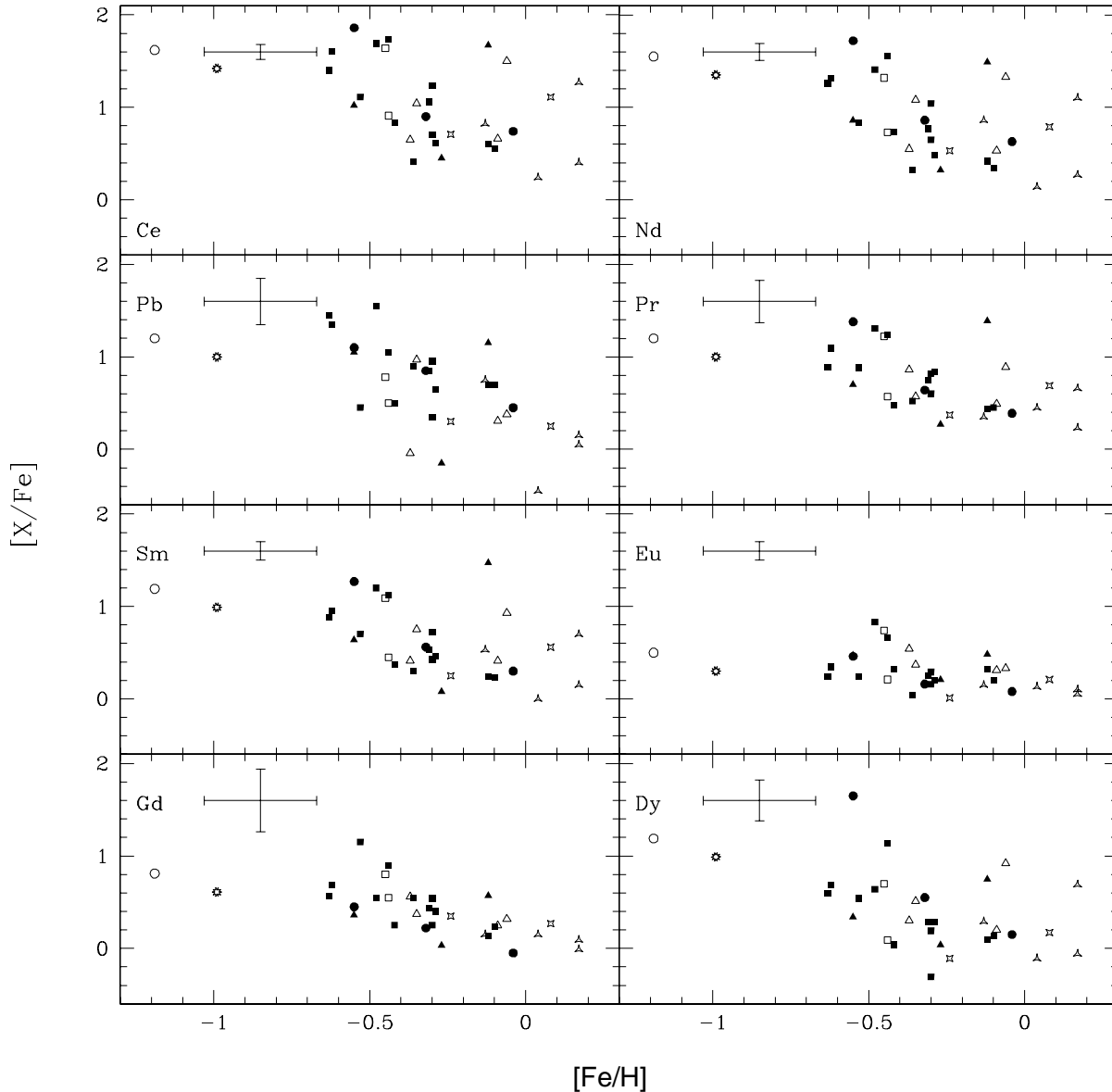


Fig. 14. $[X/Fe]$ vs. $[Fe/H]$ for heavy elements. Symbols are the same as in Figure 11.

(see Figure 12), in agreement with previous work (McWilliam 1997; François et al. 2004).

Zinc: Sneden & Crocker (1988) and Sneden et al. (1991) obtained a constant behaviour for Zn with $[Zn/Fe] = 0$, and this result was confirmed by Mishenina et al. (2002) for $[Fe/H] > -2.0$. Cayrel et al. (2004) observed an increasing trend of $[Zn/Fe]$ toward lower metallicities. The results of Cayrel et al. (2004) are shown in Figure 5 of François et al. (2004), including also observations from previous work, showing that for $[Fe/H] > -2.5$, $[Zn/Fe]$ is approximately constant, although with a dispersion in the range $-0.25 \leq [Zn/Fe] \leq 0.3$.

Similarly to Cu, Zn can be produced by a sum of nucleosynthetic processes (Mishenina et al. 2002), the weak component

of the s-process (Sneden et al. 1991), SN Ia (Matteucci et al. 1993) and SN II (Timmes et al. 1995).

In the present work, 4 atomic lines were used in order to compute Zn abundance. Generally, the results derived from different lines are in good agreement. For 6 stars a larger difference was observed from 0.25 to 0.6 dex, usually between the lines $\lambda 4680.1 \text{ \AA}$ and $\lambda 6362.3 \text{ \AA}$. This difference should not be due to atomic constants, once for most stars a good agreement was found. $[Zn/Fe]$ vs. $[Fe/H]$ shown in Figure 12 is in good agreement with François et al. (2004).

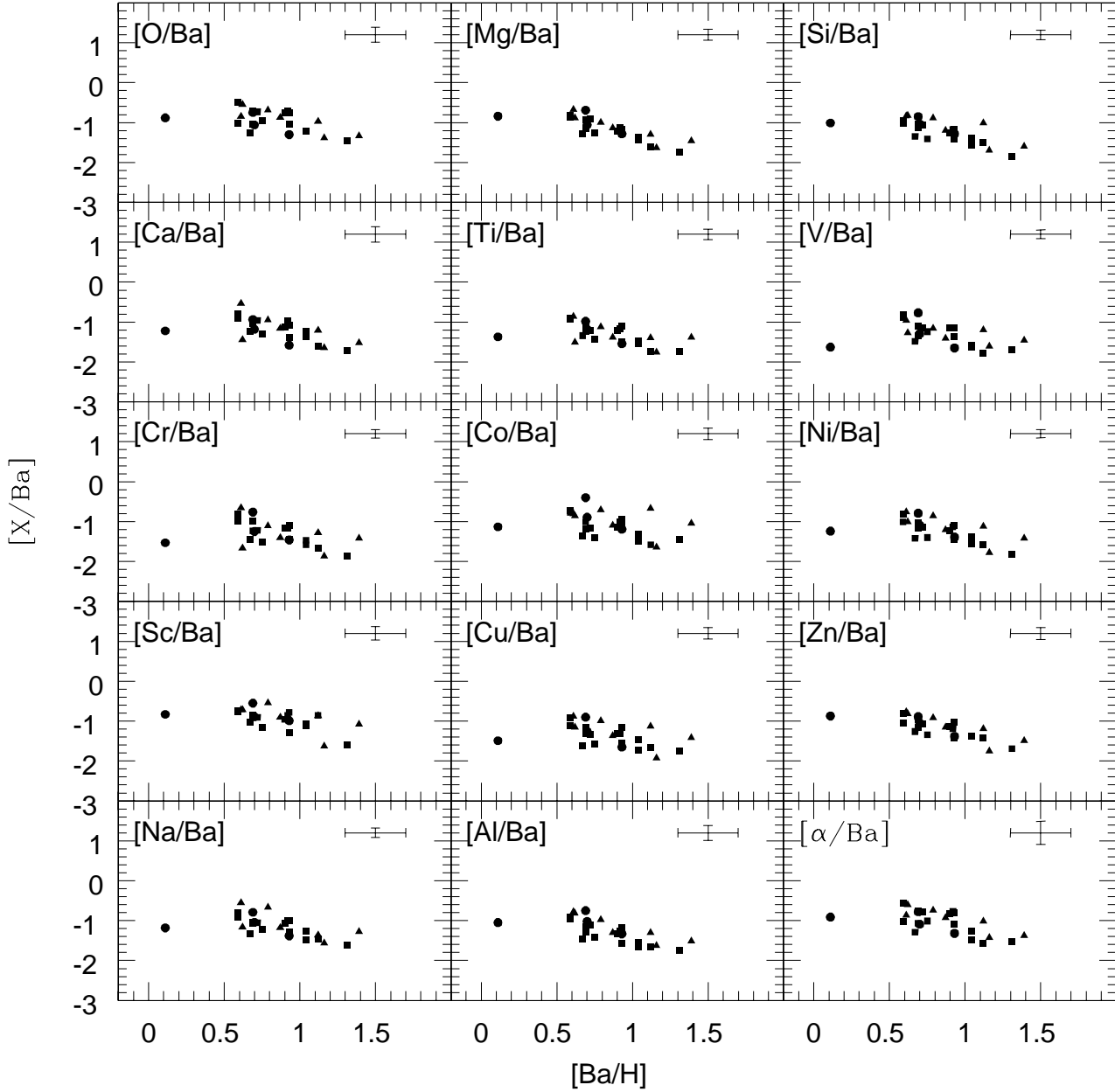


Fig. 15. $[X/Ba]$ vs. $[Ba/H]$. Symbols: squares: dwarf stars ($\log g \geq 3.7$); triangles: subgiants ($2.4 < \log g < 3.7$); circles: giants ($\log g \leq 2.4$).

4.7. s-elements

In the s-elements list we included those elements that have more than 50% of s-process contribution for their abundances, according to Arlandini et al. (1999). Molybdenum was also included in this list, given that the s-process contribution for its abundance, although lower than 50%, is much larger than r- and p-processes. Details of the s-, r- and p-processes contributions for heavy elements abundances of sample stars will be found in the forthcoming paper by Allen & Barbuy (2006, paper II).

Strontium: Few studies on strontium are found. Mashonkina & Gehren (2001) found $-0.2 \leq [Sr/Fe] \leq 0.1$ for disk stars in the range of metallicities $-1.5 \leq [Fe/H] \leq 0$. For one star of the sample with $[Fe/H] \approx -1$ they found $[Sr/Fe] \approx 0.2$. In the same range of metallicities, Gratton & Sneden (1994) found $-0.2 \leq [Sr/Fe] \leq 0.2$. Jehin et al. (1999) obtained $-0.4 < [Sr/Fe] < 0$ in the metallicity range $-1.3 \leq [Fe/H] \leq -0.8$.

The difficulty in computing Sr abundance is the strength of the line $\lambda 4077.7 \text{ \AA}$, which characterises barium stars. However, for most stars the abundance derived from this line was very close to that from $\lambda 4161.8 \text{ \AA}$, as shown in Table 15. The larger

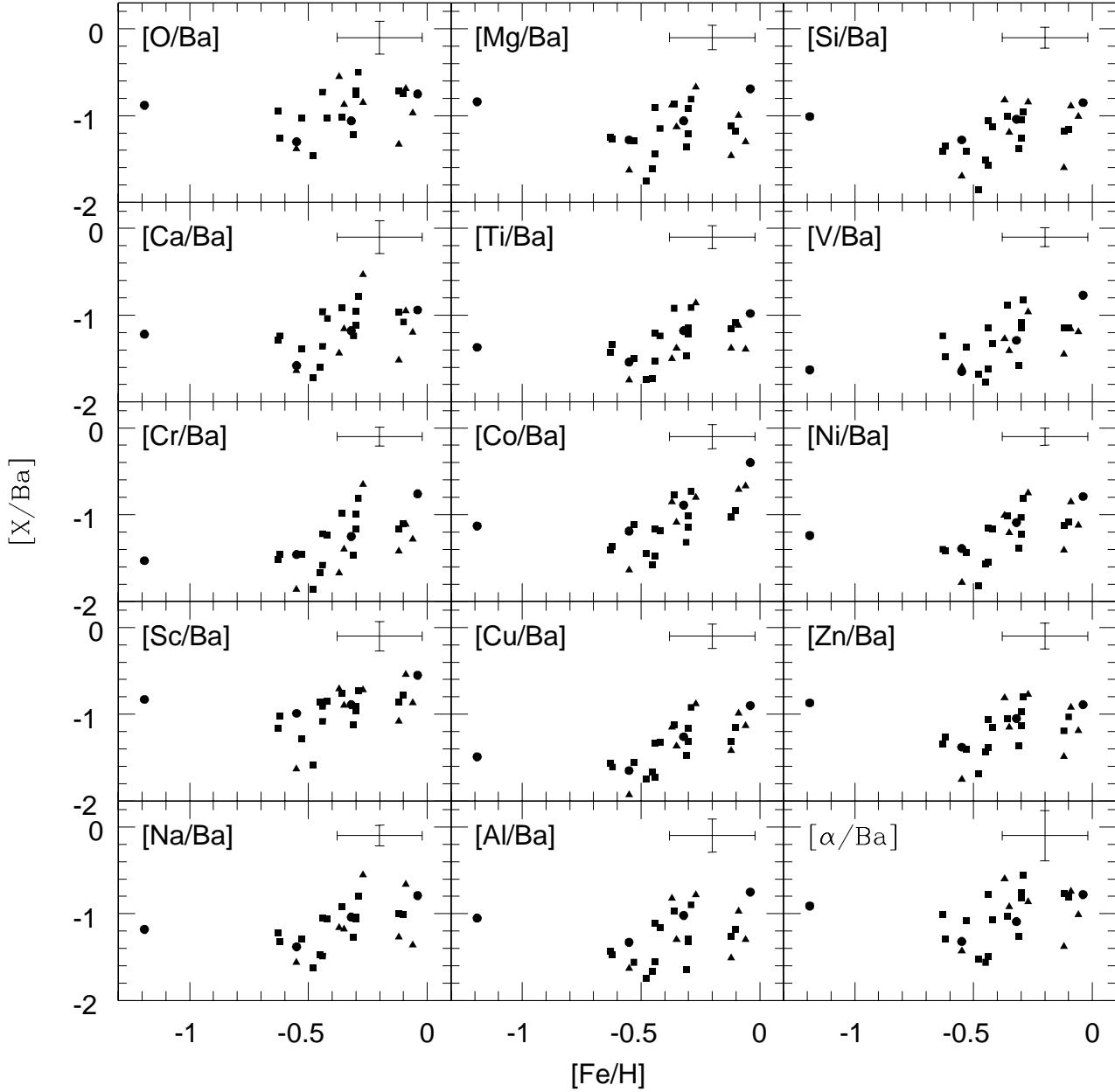


Fig. 16. $[X/Ba]$ vs. $[Fe/H]$. Symbols are the same as in Figure 15.

difference is for HD 147609 (0.80 dex) followed by HD 12392 (0.45 dex) and HD 188985 (0.30 dex). Lines of Sr I usually result in lower abundances than Sr II ones. This effect is also seen in the solar abundances computed by Gratton & Sneden (1994). Figure 13 shows that the relation $[Sr/Fe]$ vs. $[Fe/H]$ presents a larger dispersion for Sr II than for Sr I. Most data are in the range $0.6 \leq [Sr II/Fe] \leq 1.40$ and $0.3 \leq [Sr I/Fe] \leq 1.2$.

Yttrium: Gratton & Sneden (1994), Jehin et al. (1999), Tomkin & Lambert (1999) and Edvardsson et al. (1993) found an increasing trend of $[Y/Fe]$ toward higher metallicities, excluding the peculiar stars in their samples. In the present work, Y abundance was computed using synthesis of 12 lines of

Y II. In general the results derived from different lines are in good agreement. A few lines result in different abundances that can reach 0.7 dex for some stars, as can be seen in Table 15. The gf-values for the lines of Y II were those from Hannaford et al. (1982), except for the line $\lambda 6795.4 \text{ \AA}$, with log gf from McWilliam & Rich (1994). The gf-values from Hannaford et al. (1982) were also used by Gratton & Sneden (1994) resulting in $\log \epsilon_{\odot}(Y) = 2.21 \pm 0.02$ for the solar abundance, in agreement with Grevesse & Sauval (1998) value of $\log \epsilon_{\odot}(Y) = 2.24 \pm 0.03$. Gratton & Sneden (1994) obtained $-0.3 \leq [Y/Fe] \leq 0.1$ at $[Fe/H] \approx -1$, and $[Y/Fe] \approx 0$ at $[Fe/H] \approx -0.3$. Tomkin & Lambert (1999) found $-0.2 \leq [Y/Fe] \leq 0$ in the

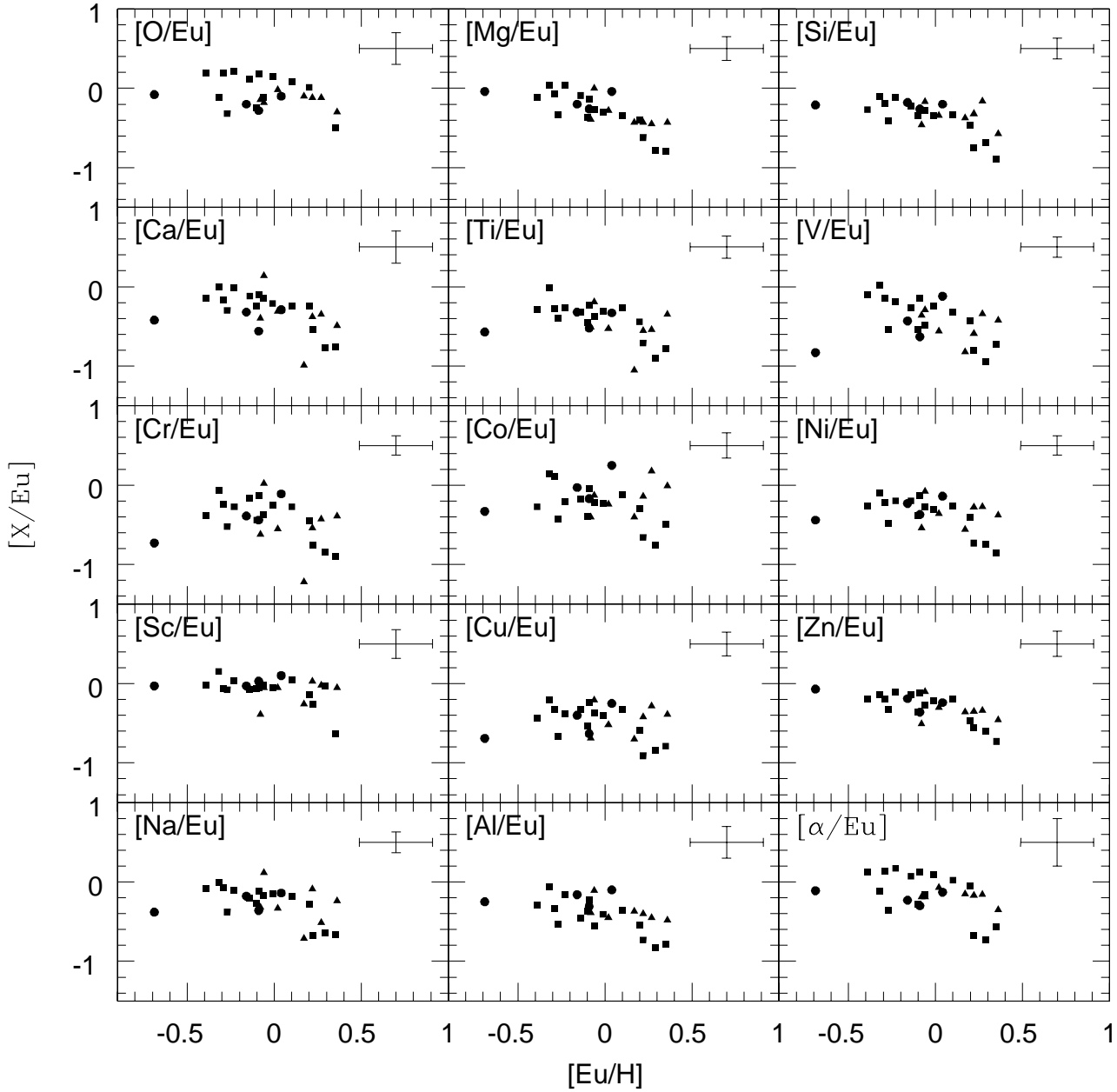


Fig. 17. $[X/Eu]$ vs. $[Eu/H]$. Symbols are the same as in Figure 15.

range $-1 \leq [Fe/H] \leq 0$. Figure 13 shows resulting values much higher for the present barium stars, in the range $0.50 \leq [Y/Fe] \leq 1.60$.

Zirconium: a combination of results by Burris et al. (2000, and references therein), Gratton & Sneden (1994) and Tomkin & Lambert (1999) gives a relation of $[Zr/Fe]$ vs. $[Fe/H]$ similar to those of Sr and Y. The dispersion increases for $[Fe/H] < -1.5$, whereas for higher metallicities, $[Zr/Fe]$ is in the range $-0.2 \leq [Zr/Fe] \leq 0.5$. For the sample barium stars the dispersion is also present, and the values are much higher than for normal stars. Table 15 shows that the abundances derived from Zr I are usually lower than those from Zr II in the range 0.40

$\leq [Zr \text{ II}/Fe] \leq 1.60$ and $-0.20 \leq [Zr \text{ I}/Fe] \leq 1.45$, the latter with higher dispersion, as shown in Figure 13.

Sr, Y and Zr form the first peak of abundance of the s-process. The reason is that they have one isotope with a neutron magic number ($N=50$), ^{88}Sr , ^{89}Y and ^{90}Zr . The larger contribution for the abundance of those elements comes from those isotopes. Figure 13 shows that $[Sr, Y, Zr/Fe]$ vs. $[Fe/H]$ are far higher than $[Mo/Fe]$ vs. $[Fe/H]$. Some stars show deficiency in Mo that can reach -0.20 .

Molybdenum: According to Arlandini et al. (1999), the Mo abundance in the solar system has a contribution of 49.76% from s-process, 26.18% from r-process and 24.06% from p-

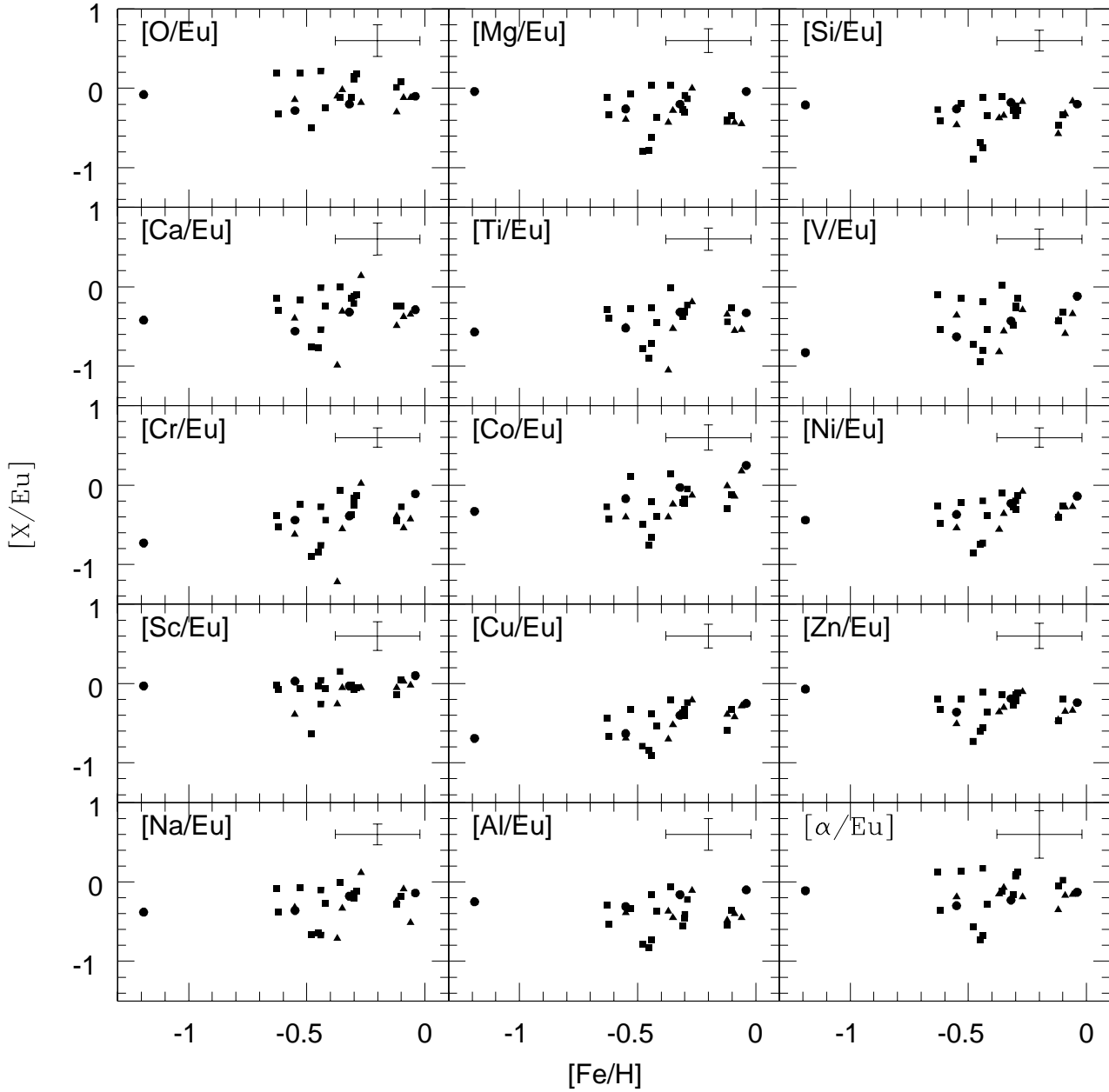


Fig. 18. $[X/Eu]$ vs. $[Fe/H]$. Symbols are the same as in Figure 15.

process. For the latter process, Mo is responsible for an abundance peak.

In the present sample, only the line $\lambda 5570.4 \text{ \AA}$ was available, for which the $\log gf$ from Biémont et al. (1983) was used. For the same line and $\log gf$, Smith et al. (2000) obtained 1.97 for the solar abundance, close to the value by Grevesse & Sauval (1998) of 1.92 ± 0.05 .

Mo is little studied. Smith et al. (2000) obtained $-0.21 \leq [Mo/Fe] \leq 0.9$ for a sample of 10 red giant stars from the globular cluster ω Centauri, in the range $-1.8 \leq [Fe/H] \leq -0.8$. The range $-0.20 \leq [Mo/Fe] \leq 1.0$ was obtained for the stars

of the present sample, showing a much lower pattern than the s-elements, as shown in Figure 13.

Barium: Spite & Spite (1978) verified that $[Ba/Fe]$ increases in the range $-3 < [Fe/H] \leq -1.5$, that they called as “halo enrichment”. For $[Fe/H] > -1.5$ the Ba enrichment is very slow, or null. This effect is confirmed by Burris et al. (2000, and references therein), Gratton & Sneden (1994), Mashonkina & Gehren (2001) and Tomkin & Lambert (1999), which show $[Ba/Fe]$ increasing to values close to solar abundance in the range $-4 \leq [Fe/H] \leq -2$, and values $-0.4 \leq [Ba/Fe] \leq 0.4$ for $[Fe/H] > -2$.

13), showing the large La overabundance relative to Fe for barium stars, in contrast to normal stars.

Cerium: Gratton & Sneden (1994) and Jehin et al. (1999) showed for [Ce/Fe] a behaviour similar to [Ba/Fe] and [La/Fe]. Their results are in the range $-0.4 \leq [\text{Ce/Fe}] \leq 0.15$ for $-2 \leq [\text{Fe/H}] \leq 0$. In the present work, 8 lines of Ce II were used for abundance determination. As for La, in some cases, the abundance result of one line was very different from the others, but the effect on the average is low, as can be seen in Table 15, 16 and 17. Abundance excess relative to Fe is in the range $0.4 \leq [\text{Ce/Fe}] \leq 1.80$, with large dispersion among the stars.

Neodymium: Gratton & Sneden (1994), Tomkin & Lambert (1999), Jehin et al. (1999) and Burris et al. (2000, and references therein) show that [Nd/Fe] behaves similarly to Ba, La and Ce. According to Figure 5 from Burris et al. (2000), a high dispersion in the range $-3 \leq [\text{Fe/H}] \leq -1.5$ is present, with low values close to $[\text{Nd/Fe}] \approx -0.6$ and high values of $\approx +1.5$. For $[\text{Fe/H}] > -1.5$ the results are in the range $-0.3 \leq [\text{Nd/Fe}] \leq +0.3$.

In the calculation of Nd abundance for the present sample, the hyperfine structure was neglected. According to Hartog et al. (2003), only the odd isotopes ^{143}Nd and ^{145}Nd show hyperfine structure, accounting for 20.5% of the abundance, hence the effect can be ignored. The abundances derived from 9 lines of Nd II were computed, and they show a good agreement, with a few exceptions, similar to previous elements described here. The range obtained for the abundance excess relative to Fe was $0.3 \leq [\text{Nd/Fe}] \leq 1.70$.

Ba, La, Ce and Nd form the second abundance peak of the s-process because of nuclides ^{138}Ba , ^{139}La , ^{140}Ce and ^{142}Nd are neutron magic nuclei ($N=82$).

Lead: There are a few stars for which the lead abundance was determined. Van Eck et al. (2003), show that some CH stars show high Pb abundances, and Sivarani et al. (2004) gathered about 30 halo stars with high Pb abundances. There are 4 Pb isotopes: ^{204}Pb , ^{206}Pb , ^{207}Pb and ^{208}Pb . The last is doubly magical (neutron magic in $N=126$ and proton magic in $Z=82$) being the responsible for the third abundance peak of the s-process. The best lines for the abundance calculation are $\lambda 3639.6 \text{ \AA}$, $\lambda 3683.5 \text{ \AA}$, $\lambda 3739.9 \text{ \AA}$, $\lambda 4057.8 \text{ \AA}$ and $\lambda 7229 \text{ \AA}$. Wavelengths $\lambda < 4000 \text{ \AA}$ are not reliable with the FEROS spectra and the $\lambda 7229 \text{ \AA}$ line is too weak. For these reasons, the Pb abundance was determined using the line $\lambda 4057.8 \text{ \AA}$, for which blends have been taken into account. The results are in the range $-0.2 \leq [\text{Pb/Fe}] \leq 1.6$, showing a large dispersion. According to Arlandini et al. (1999), the s-process is responsible for 46% of the Pb abundance with no contribution from the r-process. The missing abundance is generally attributed to the strong component of the s-process.

4.8. r-elements

We included in the r-elements list only those with more than 50% of r-process contribution for their abundances, according to Arlandini et al. (1999).

Europium: Gratton & Sneden (1994), Burris et al. (2000), Jehin et al. (1999), Woolf et al. (1995) and

Mashonkina & Gehren (2001) provide an increasing linear relation between $\log \epsilon(\text{Eu})$ and $[\text{Fe/H}]$. On the other hand, $[\text{Eu/Fe}]$ decreases toward higher metallicities.

In the present work the lines $\lambda 4129.7 \text{ \AA}$, $\lambda 4205 \text{ \AA}$, $\lambda 6437.7 \text{ \AA}$ and $\lambda 6645.1 \text{ \AA}$ were used for computing Eu abundances, taking into account the hyperfine structure. The abundances derived from these 2 first lines are usually lower than those derived from the 2 last lines (see Table 15). The 2 first lines show a blend with CN lines in the cooler stars, whereas for the hotter stars, this blend is negligible.

Figure 17 and Table 18 show the relation between $[\text{Eu/H}]$ and abundance excess of α - and iron peak elements relative to Eu, showing a larger dispersion than Figure 15. With the exception of O, Mg, Co and Sc, the other α - and iron peak elements show $[\text{X/Eu}] \leq 0$. It seems that there is an interval of $[\text{Eu/H}]$ where $[\text{X/Eu}]$ is constant and, for $[\text{Eu/H}] > 0$ a decreasing trend is seen, that could reflect the secondary character of the r-process with the iron peak elements as the seed nuclei. A primary r-process (e.g. Meyer 1994) contribution would form Eu without depletion of other elements. Relative to $[\text{Fe/H}]$ (Figure 18), $[\text{X/Eu}]$ seems to be constant, with the possible exception of $[\text{Cr/Eu}]$, $[\text{Co/Eu}]$ and $[\text{Cu/Eu}]$ which seem to increase toward increasing metallicities. The constancy of $[\text{X/Fe}]$ could be due to the fact that α -elements, and probably Na and Al, are produced in massive stars (mostly in hydrostatic phases), and they are released in their SNaE type II explosions as well as the r-elements. Thus, if all of them were released through the same events, their ratios are expected to be constant. The dispersion comes from the fact that stars of different masses produce different amounts of each element. Regarding the increasing or constant behaviour of $[\text{iron peak/Eu}]$ vs. $[\text{Fe/H}]$, it can be due to their production in different amounts in SNaE II and SNaE Ia. A larger range of metallicities expanded toward lower values could illustrate better such behaviour.

Praseodymium: Little is done on Pr. Gratton & Sneden (1994) determined Pr abundance for metal-poor stars and obtained results in the range $-0.2 \leq [\text{Pr/Fe}] \leq 0.3$, for $-1.5 \leq [\text{Fe/H}] \leq 0$. Figure 14 shows that the present results are in the range $0.2 \leq [\text{Pr/Fe}] \leq 1.40$, showing the contribution of the s-process to the Pr abundance. The three lines used were in good internal agreement, with a few exceptions, as shown in Table 15.

Samarium: Gratton & Sneden (1994) included Sm in their analysis with results in the range $-0.3 \leq [\text{Sm/Fe}] \leq 0.2$ for $-1.5 \leq [\text{Fe/H}] \leq 0$. In the present work, the results are in the range $0 \leq [\text{Sm/Fe}] \leq 1.40$ (Figure 14).

The Sm lines are very weak and the hfs of the 5 lines can be neglected. The abundances derived from several lines are in good agreement, as can be seen in Table 15.

Gadolinium: Gadolinium abundances are essentially not found in the literature, at least, in the range of metallicities of the present sample. The lines are very weak or even invisible in the spectra. Furthermore, they are only present at $\lambda < 5000 \text{ \AA}$ with several blends.

In the present work 3 lines of Gd were used. For most of them there was good agreement among the abundances derived from different lines (see Table 15). Figure 14 shows low dispersion in the relation $[\text{Gd/Fe}]$ vs. $[\text{Fe/H}]$.

Dysprosium: Gratton & Sneden (1994) studied stars in the range of metallicities $-1.5 \leq [\text{Fe}/\text{H}] \leq 0$, and they included Dy in their analysis. They found a range of $-0.2 \leq [\text{Dy}/\text{Fe}] \leq 0.2$ except for one star for which they found $[\text{Dy}/\text{Fe}] \approx -0.4$. The results of the present sample are in the range of $-0.25 \leq [\text{Dy}/\text{Fe}] \leq 1.65$, shown in Figure 14. Two lines were available in the spectra of the sample stars, from which a good agreement was obtained.

4.9. Uncertainties

The abundance uncertainties were calculated by verifying how much the variation of each input parameter changes the output value $\log A_p$. Table 19 shows the values taken into account in this calculation and the resulting uncertainties for each element. The procedure was adopted for 2 stars, HD 5424 of low $\log g = 2.0$ and HD 150862 of high $\log g = 4.6$.

The uncertainty on the output value is given by

$$\sigma_{A_p} = \sqrt{(\Delta A_T)^2 + (\Delta A_{lg})^2 + (\Delta A_v)^2 + (\Delta A_m)^2} \quad (14)$$

where ΔA_T , ΔA_{lg} , ΔA_v and ΔA_m are the differences in A_p due to variations of 1σ in the temperature, $\log g$, microturbulent velocity and metallicity, respectively.

The average value of A_p (A_{pm}) is obtained by averaging individual abundances of several lines, and not from several measurements of the same line. In the latter case, the standard deviation could be used to calculate the uncertainty on A_{pm} . Considering this, we found more suitable to apply propagation of errors taking into account the uncertainty calculated with equation 14. Thus, the uncertainty on A_{pm} is

$$\sigma_{A_{pm}} = \frac{\sigma_{A_p}}{\sqrt{n}} \quad (15)$$

where n is the number of lines. The uncertainty on the logarithm of A_{pm} is

$$\sigma_{\log(A_{pm})} = \frac{\sigma_{A_{pm}}}{A_{pm} \ln 10}. \quad (16)$$

The abundance $\log \epsilon(X)$ is related to the output of the synthesis program by $\log \epsilon(X) = \log A_{pm} + [\text{Fe}/\text{H}]$. Therefore, the uncertainty is

$$\sigma_{\log \epsilon(X)} = \sqrt{\sigma_{\log(A_{pm})}^2 + \sigma_{[\text{Fe}/\text{H}]}^2}. \quad (17)$$

The relation between the abundance excess relative to iron $[X/\text{Fe}]$ and the output value of the synthesis program is $[X/\text{Fe}] = \log A_{pm} - \log \epsilon(X)_\odot$, where $\log \epsilon(X)_\odot$ is the solar abundance of the element “X”. The uncertainty is calculated by

$$\sigma_{[X/\text{Fe}]} = \sqrt{\sigma_{\log(A_{pm})}^2 + \sigma_{\log \epsilon_\odot(X)}^2} \quad (18)$$

The uncertainty on $[\alpha/\text{Fe}]$, which contains the contribution of the uncertainty on the abundance of each element taken into account in the calculation of the α 's, is given by

$$\sigma_{[\alpha/\text{Fe}]} = \sqrt{\sigma_{\log \epsilon(\alpha)}^2 + \sigma_{\log \epsilon_\odot(\alpha)}^2 + \sigma_{[\text{Fe}/\text{H}]}^2} \quad (19)$$

with

$$\sigma_{\log \epsilon(\alpha)} = \frac{1}{n \epsilon(\alpha)} \sqrt{\sum_{i=1}^n (10^{\log \epsilon(X_i)})^2 \sigma_{\log \epsilon(X_i)}^2} \quad (20)$$

where n is the number of elements “X” used in the calculation of α , $\epsilon(\alpha) = 10^{\log \epsilon(\alpha)}$. In this work, $n=5$ for most stars. For 2 stars, HD 87080 and HD 147609, $n=4$ because the oxygen was excluded from the calculation. The $\sigma_{\log \epsilon(\alpha)_\odot}$ is similar to expression 20.

For the iron peak elements, the uncertainty is similar to expression 19.

In Figures 4, 5, 6, 7, 8, 9, 10, 11, 12, 13, 17, 18 are shown the maximum value of uncertainties on each axis. In the corresponding tables it is possible to check all the values.

5. Conclusions

The barium stars have been studied throughout more than five decades, however several open questions still remain relative to their origin and characteristics. The aim of the present work was to increase the knowledge about this class of peculiar stars.

For the first time a detailed study on the behaviour of abundance ratios for a large number of elements is presented for a relatively large sample of barium stars.

As the first outcome of this work, the results of the atmospheric parameters show that the sample consisted of stars of different luminosity classes with $4300 \leq T_{eff} \leq 6500$ K and $1.4 \leq \log g \leq 4.6$.

The metallicities obtained are typical of barium stars, in the range $-1.2 \leq [\text{Fe}/\text{H}] \leq 0.0$, most of them with $-0.62 \leq [\text{Fe}/\text{H}] \leq 0.0$.

For 7 stars a significant difference was found between the metallicities resulting from Fe I and Fe II lines, ($\Delta[\text{Fe}/\text{H}] \geq 0.2$ dex). It is very important this to be understood in order to be possible to determine reliable abundances, given that the errors in metallicities affect the resulting abundances. The difference appears when one determines the surface gravities through the classical equation, which requires the mass values. In the present work, two methods were adopted. In the first case, the masses were derived from isochrones and then the surface gravities were determined. In the second case, the surface gravities were derived from ionization equilibrium and then the masses. The difference between the surface gravities determined from the two methods can reach 0.6 dex and in the worst case, over 1 dex for the star HD 147609. This difference reflects in the differences between the metallicities derived from lines of Fe I and Fe II. One point to discuss is the fact that the masses determined using the $\log g$ from ionization equilibrium are very small for these 7 stars. Another point is that $\Delta[\text{Fe}/\text{H}]$ depends on the gf-values adopted (see Sect. 3.5). Fe II lines are less affected by NLTE effects than Fe I, and more accurate gf-values for Fe II lines were used (Meléndez & Barbuy 2006), reducing the difference in $\log g$ by 0.2 dex.

There is a good agreement between the present results and literature data. The abundance results obtained for the sample stars show that there are no correlations with the luminosity classes. The abundances found for the α -, iron peak, Li, Al and

Na are compatible with the values of $[X/Fe]$ given in the literature for normal disk stars in the same range of metallicities, and the *s*-overabundance is independent of luminosity class. There are not enough halo stars in the present sample to identify differences between halo and disk barium stars. The range of metallicities is too small to allow a well-defined trend in the $[X/Fe]$ vs. $[Fe/H]$ of α - and iron peak elements. For heavy elements, there is a small variation that can be explained by the variable amount of enriched material that each star received from the more evolved companion.

The Li abundance decreases toward lower temperatures. This result is consistent with the discussion in the literature that the Li is depleted along the red giant branch evolution.

Less evolved stars show higher C abundances, and $[C/O]$ is approximately constant with metallicity. Besides being C-rich, the barium stars of the present sample are N-rich. It happens for all stars including the less evolved ones, suggesting that N is also responsible for the CNO excess in these stars.

For most stars, the excesses of Na, Al, Mg, Si and Ca relative to Fe are within $-0.2 < [X/Fe] < 0.2$. O reaches higher values and Ti, lower values. $[Ti/Fe]$ are approximately similar to those of $[V/Fe]$, $[Cr/Fe]$ and $[Ni/Fe]$, identifying Ti more as iron peak than an α -element. For some stars the odd-even effect, where Mg and Si are overabundant relative to Na and Al, can be observed, however, for several stars the abundances of Na and Al are higher than those of Si and Mg.

Among iron peak elements, the Sc has the highest abundances. This result is in agreement with Nissen et al. (2000), that identified an “ α -element” behaviour for Sc. For Co, the theoretical prediction is $[Co/Fe] < 0$ for the range of metallicities of the present sample, however, for most stars $[Co/Fe] > 0$ was obtained. For other iron peak elements, V, Cr, Ni and Zn, $[X/Fe]$ show a lower range of values than $[Co/Fe]$. Except for 4 stars, $[Cu/Fe]$ is below solar for the present sample.

The excesses of Na, Al, α - and iron peak elements relative to Ba show a decreasing trend with $[Ba/H]$, whereas $[X/Ba]$ vs. $[Fe/H]$ show an increasing trend. Considering that Ba represents the *s*-process elements, one can consider that these correlations describe the relations between *s*-process and other nucleosynthetic processes.

Regarding the *r*-process element Eu, there is a range of $[Eu/H]$ where $[X/Eu]$ is essentially constant, $[X/Eu]$ showing a decreasing trend toward higher $[Eu/H]$. For most stars, $[X/Eu] \leq 0$, except for O, Mg, Co and Sc. $[X/Eu]$ vs. $[Fe/H]$ is constant for Na, Al and α -elements as expected. $[X/Ba]$ and $[X/Eu]$ for the sample stars characterises the abundance behaviour of different elements relative to the *s*- and *r*-processes.

Acknowledgements. We acknowledge partial financial support from the Brazilian Agencies CNPq and FAPESP. DMA acknowledges a FAPESP PhD fellowship n° 00/10405-8 and a FAPERJ post-doctoral fellowship n° 152.680/2004. We are grateful to Anita Gómez for suggesting the analysis of Hipparcos dwarf barium stars candidates, to Andrew McWilliam for making available his code on hyperfine structure and to the referee, Nils Ryde, for useful comments. We are also grateful to Licio da Silva, Luciana Pompéia, Paula Coelho and Jorge Meléndez for carrying out some observations of our sample spectra, and to Gustavo Porto de Mello, Wladimir and Graziela, for helping us with photometric observations. This pub-

lication makes use of the SIMBAD database and of data products from the Two Micron All Sky Survey, which is a joint project of the University of Massachusetts and the Infrared Processing and Analysis Center/California Institute of Technology, funded by the National Aeronautics and Space Administration and the National Science Foundation.

References

- Allen D.M., Barbuy B., 2006, A&A, submitted (paper II)
 Allende Prieto C., Garcia-Lopez R., Lambert D.L., Gustafsson B. 1999, ApJ, 527, 879
 Allende Prieto C., Lambert D.L., Asplund M., 2001, ApJ 556, L63
 Alonso A., Arribas S., Martinez-Roger C., 1995, A&A, 297, 197
 Alonso A., Arribas S., Martinez-Roger C. 1996, A&A 313, 873
 Alonso A., Arribas S., Martinez-Roger C. 1999, A&AS 140, 261
 Andersson H., Edvardsson B. 1994, A&A, 290, 590
 Arlandini C., Käppeler F., Wisshak K. 1999, ApJ, 525, 886
 Arnett W.D. 1971, ApJ, 166, 153
 Asplund M., Grevesse N., Sauval J. 2005, astro-ph/0410214
 Baraffe I., Takahashi K. 1993, A&A, 280, 476
 Barbuy B., 1988, A&A, 191, 121
 Barbuy B., Jorissen A., Rossi S.C.F., Arnould M. 1992, A&A, 262, 216
 Barbuy B., Perrin, M.-N., Katz, D., Coelho, P., Cayrel, R., Spite, M., Van't Veer-Menneret, C., 2003, A&A, 404, 661
 Barbuy B., Renzini A., Ortolani S., Bica E., Guarnieri M.D., 1999, A&A, 341, 539
 Barklem P.S., O'Mara B.J., Ross J.E., 1998, MNRAS, 296, 1057
 Barklem P.S., Piskunov, N., O'Mara, B. J., 2000, A&AS, 142, 467
 Baumüller D., Butler K., Gehren T. 1998, A&A, 338, 637
 Baumüller D., Gehren T. 1997, A&A, 325, 1088
 Bell R.A., Eriksson K., Gustafsson B., Nordlund A., 1976, A&AS 23, 37
 Bergstrom H., Biémont E., Lundberg H., Persson A., 1988, A&A, 192, 337
 Bertelli G., Bressan A., Chiosi C., Fagotto F., Nasi E., 1994, A&AS, 106, 275
 Bessell M.S. 1979, PASP 91, 589
 Bessell M.S., Brett J.M. 1988, PASP 100, 1134
 Bessell M.S., Castelli, F., Plez, B. 1998, A&A 333, 231
 Bidelman W.P., Keenan P.C. 1951, ApJ 114, 473
 Biehl D., 1976, Ph.D. Thesis, Kiel University
 Bielski, A. 1975, JQSRT, 15, 463
 Biémont E. Gamir H.P., Palmeri P., Li Z.S., Svanberg S., 2000, MNRAS, 312, 116
 Biémont E., Godefroid M., 1980, A&A, 84, 361
 Biémont E., Grevesse N., Hannaford P., Lowe R.M., 1981, ApJ, 248, 867
 Biémont E., Grevesse N., Hannaford P., Lowe R.M. 1989, A&A, 222, 307
 Biémont E., Grevesse N., Hannaford P., Lowe R.M., Whaling W. 1983, ApJ, 275, 889

- Biémont E., Lowe R.M. 1993, A&A, 273, 665
- Boesgaard A.M. 1970, ApJ, 161, 1003
- Bond H.E., Neff I.S., 1969, ApJ, 158, 1235
- Bond H.E., Pollacco D.L., Webbink R. 2003, ApJ, 125, 260
- Böhm-Vitense E. 1980, ApJ, 239, L79
- Böhm-Vitense E., Carpenter K., Robinson R., Ake T., Brown J. 2000, ApJ, 533, 969
- Böhm-Vitense E., Johnson H.R. 1985 ApJ, 293, 288
- Brown J.A., Sneden C., Lambert D.L., Dutchover E. 1989, ApJS, 71, 293
- Burris, D.L., Pilachowski C.A., Armandroff T.E., Sneden C., Cowan J.J., Roe H. 2000, ApJ, 544, 302
- Cardelli J.A., Clayton G.C., Mathis J.S. 1989, ApJ 345, 245
- Carpenter J.M. 2001, AJ 121, 2851
- Castilho B.V., Gregorio-Hetem J., Spite F., Spite M., Barbuy B. 1998, A&AS, 127, 139
- Castilho B.V., Pasquini L., Allen D.M., Barbuy B., Molaro P., 2000, A&A, 361, 92
- Catchpole R.M., Robertson B.S.C., Warren P.R., 1977, MNRAS, 181, 391
- Cayrel, R., 1989, em *The impact of very high S/N spectroscopy on stellar physics*, ed. G. Cayrel de Strobel, & M. Spite (Dordrecht: Kluwer Academic Publ.), IAU Symp., 132, 345
- Cayrel, R., Depagne E., Spite M., et al. 2004, A&A, 416, 1117
- Cayrel, R., Jugaku, 1963, AnAp, 26, 495
- Cayrel, R., Perrin M.N., Barbuy B., Buser R., 1991, A&A, 247, 108
- Chen, B., Vergely J.L., Valette B., Carraro G. 1998, A&A 336, 137
- Clegg R.E.S., Lambert D.L., Tomkin J. 1981, ApJ, 250, 262
- Coelho P., Barbuy, B., Meléndez, J., Schiavon, R.P., Castilho, B.V. 2005, A&A, 443, 735
- Corliss C.H., Bozman W.R., 1962,
- Cram L. 1999 em *Transactions of the International Astronomical Union*, Volume XXIIIB, 141, Editor: J. Andersen
- Cutri R.M., Skrutskie M.F., van Dyk S., et al. 2003, VizieR Online Data Catalog, 2246
- Denn G.R., Luck R.E., Lambert D.L. 1991, ApJ, 377, 657
- Dominy J.F., Lambert D.L. 1983, ApJ, 270, 180
- Domogatskii G.V., Eramzhyan R.A., Nadyozhin D.K. 1977, em *Neutrino 77* (Nauka, Moscow), p. 115
- Edvardsson B., Andersen J., Gustafsson B., Lambert D.L., Nissen P.E., Tomkin J. 1993, A&A, 275, 101
- François P., Matteucci F., Cayrel R., Spite M., Spite F., Chiappini C. 2004, A&A, 421, 613
- Fuhrmann K., Axer M., Gehren T., 1995, A&A, 301, 492
- Goly A., Kusz J., Nguyen Quang B., Weniger S., 1991, JQSRT, 45, 157
- Gómez A.E., Luri X., Grenier S., Prévot L., Mennessier M.O., Figueras F., Torra J. 1997, A&A 319, 881
- Goswami, A., Prantzos, N. 2000, A&A, 359, 191
- Gratton R.G., Carreta E., Castelli F., 1996, A&A, 314, 191
- Gratton R.G., Sneden C. 1991, A&A, 241, 501
- Gratton R.G., Sneden C. 1994, A&A, 287, 927
- Grevesse N., Sauval A.J. 1998, Space Sci. Rev., 85, 161
- Gustafsson B., Bell K.A., Eriksson K., Nordlund Å., 1975, A&A, 42, 407
- Hakkila J., 1989, A&A, 213, 204
- Hannaford P., Lowe R.M., Grevesse N., Biémont E., Whaling W. 1982, ApJ, 261, 736
- Hannaford P., Lowe R.M., 1983, Opt. Eng, 22, 532
- Hartog E.A.D., Lawler J.E., Sneden C., Cowan J.J. 2003, ApJS, 148, 543
- Jacoby G.H. 1981, ApJ, 244, 903
- Jasniewicz G., Thévenin F., Monier R., Skiff B. 1996, A&A, 307, 200
- Jeffries R.D., Smalley B. 1996, A&A, 315, L19
- Jehin E., Magain P., Neuforge C., Noels A., Parmentier G., Thoul A.A. 1999, A&A, 341, 241
- Kipper T., Wallerstein G. 1990, PASP, 102, 574
- Kraft R.P., Ivans I.I. 2003, PASP, 115, 143
- Kurucz R. L., Furenlid I., Brault J., 1984, Solar flux atlas from 296 to 1300 nm, National Solar Observatory Atlas, Sunspot (New Mexico: National Solar Observatory)
- Kusz J., 1992, A&AS, 92, 517
- Lage C.S., Whaling W. 1976, JQSRT, 16, 537
- Lambert D.L., 1978, MNRAS, 182, 249
- Lawler J.E., Bonvallet G., Sneden C. 2001a, ApJ, 556, 452
- Lawler J.E., Dakin J.T. 1989, J.Opt.Soc.Am., B6, 1457
- Lawler J.E., Wickliffe M.E., Hartog A.D. 2001b, ApJ, 563, 1075
- Lejeune T., Cuisinier F., Buser R. 1998, A&AS 130, 65
- Liang Y.C., Zhao G., Chen Y.Q., Qiu H.M., Zhang B. 2003, A&A, 397, 257
- Lodders K., 2003, ApJ, 591, 1220
- Lu, P.K. 1991, AJ, 101, 2229
- Luck R.E., Bond H.E., 1991, ApJS, 77, 515
- Maier R.S., Whaling W., 1977, JQSRT, 18, 501
- Martin, W.C., Fuhr, J.R., Kelleher, D.E., et al. 2002, NIST Atomic Database (version 2.0), <http://physics.nist.gov/asd>. National Institute of Standards and Technology, Gaithersburg, MD.
- Martin G.A., Fuhr J.R., Weise W.L. 1988, J.Phys.Chem.Ref.D, Vol 17, No. 3
- Mashonkina L., Gehren T. 2001, A&A, 376, 232
- Matteucci F., Raiteri C.M., Busso M., Gallino R., Gratton R. 1993, A&A, 272, 421
- McClure R.D. 1983, ApJ, 268, 264
- McClure R.D. 1984, PASP, 96, 117
- McClure R.D., Fletcher J.M., Nemeč J. 1980, ApJ, 238, L35
- McWilliam A. 1997, ARA&A, 35, 503
- McWilliam A., 1998, AJ, 115, 1640
- McWilliam A., Preston G.W., Sneden C., Searle L. 1995, AJ, 109, 2757
- McWilliam A., Rich R.M. 1994, ApJS, 91, 749
- Meléndez J., Barbuy B., 2006, in preparation
- Meléndez J., Ramirez I. 2003, A&A 398, 705
- Mennessier M.O., Luri X., Figueras F., Gómez A.E., Grenier S., Torra J., North P. 1997, A&A 326, 722
- Meyer B.S., 1994, ARA&A, 32, 153
- Mishenina T.V., Kovtyukh V.V., Soubiran C., Travaglio C., Busso M. 2002, A&A, 396, 189
- Nissen P.E., Chen Y.Q., Schuster, W.J., Zhao G. 2000, A&A, 353, 722

- Nissen P.E., Høg E., Schuster W. 1997, in *Hipparcos*, Venice '97(ESO SP-402, p. 225)
- Nomoto K., Koichi I., Nobuhiro K. 1997b, *Science*, 276, 1378
- North P., Berthet S., Lanz T. 1994, *A&A* 281, 775
- Pagel B.E.J. 1968, in *Origin and Distribution of the Elements*, ed. LH Ahrens, pp. 195-204, Oxford: Pergamon
- Palmeri P., Quinet P., Wyart J.F., Biémont E. 2000, *PhyS*, 61, 323
- Pereira C.B. 2005, *AJ*, 129, 2469
- Pereira C.B., Junqueira S. 2003, *A&A*, 402, 1061
- Perryman M. A. C., Lindegren L., Kovalevsky J. et al., 1997, *A&A*, 323, L49
- Peterson R.C., Kurucz R.L., Carney B.W. 1990, *ApJ*, 350, 173
- Plez B., Brett J.M., Nordlund A. 1992, *A&A*, 256, 551
- Przybilla, N., Butler, K., Kudritzki, R.-P. 2001, *A&A*, 379, 936
- Prochaska J.X., Naumov S.O., Carney B.W., McWilliam A., Wolfe A.M. 2000, *AJ*, 120, 2513
- Ramírez I., Meléndez J. 2004, *A&A* 417, 301
- Reddy B.E., Tomkin J., Lambert D.L., Allende Prieto C. 2003, *MNRAS*, 340, 304
- Rossi S., Beers T. C.; Sneden C., Sevcyanenko T., Rhee J., Marsteller B., 2005, *AJ*, 130, 2804
- Rutten R.J., 1978, *SoPh*, 56, 237
- Ryan S.G., Norris J.E., Beers T.C. 1996, *ApJ*, 471, 254
- Sackmann I.-J., Boothroyd A.I. 1992, *ApJ*, 392, L71
- Sackmann I.-J., Boothroyd A.I. 1999, *ApJ*, 510, 217
- Simmerer J., Sneden C., Cowan J.J., Collier J., Woolf V.M. Lawler J.E. 2004, *ApJ*, 617, 1091
- Simmerer J., Sneden C., Ivans I., Kraft R.P., Shetrone M.D., Smith V.V. 2003, *ApJ*, 125, 2018
- Sivarani, T., Bonifacio, P., Molaro, P. et al. 2004, *A&A*, 413, 1073
- Smith V.V., Coleman H., Lambert D.L. 1993, *ApJ*, 417, 287
- Smith V.V., Lambert D.L. 1986, *ApJ*, 303, 226
- Smith V.V., Suntzeff N.B., Cunha K., Gallino R., Busso M., Lambert D.L. Straniero O. 2000, *AJ*, 119, 1239
- Sneden C., Crocker D.A. 1988, *ApJ*, 335, 406
- Sneden C., Gratton R.G., Crocker D.A. 1991, *A&A*, 246, 354
- Sneden C., McWilliam A., Preston G.W., et al., 1996, *ApJ*, 467, 819
- Spite, F., Spite, M. 1975, *A&A*, 40, 141
- Spite M., Spite F. 1978, *A&A*, 67, 23
- Spite M., Spite F. 1982, *Nature*, 297, 483
- Steffen M. 1985, *A&AS*, 59, 403
- Thévenin F., 1989, *A&AS*, 77, 137
- Thévenin F., 1990, *A&AS*, 82, 179
- Thévenin F., Idiart T.P., 1999, *ApJ*, 521, 753
- Thévenin F., Jasniewicz G. 1997, *A&A*, 320, 913
- Timmes F.X., Woosley S.E., Weaver T.E. 1995, *ApJS*, 98, 617
- Tomkin J., Lambert D.L. 1999, *ApJ*, 523, 234
- Tomkin J., Lambert D.L., Edvardsson B., Gustafsson B., Nissen P.E. 1989, *A&A* 219, L15
- Udry S., Jorissen A., Mayor M., Van Eck S. 1998a, *A&AS*, 131, 25
- Udry S., Mayor M., Van Eck S., Jorissen A., Prévot L., Grenier S., Lindgren H. 1998b, *A&AS*, 131, 43
- Van Eck S., Goriely S., Jorissen A., Plez B. 2003, *A&A*, 404, 291
- Vergely J.L., Freire Ferrero R., Egret D., Köppen J. 1998, *A&A*, 340, 543
- Warner, B. 1965, *MNRAS*, 129, 263
- Woolf V.M., Tomkin J., Lambert D.L. 1995, *ApJ*, 453, 660
- Woosley S.E., Hartmann D., Hoffman R.D., Haxton W. 1990, *ApJ*, 356, 272
- Woosley S.E., Weaver T.A. 1995, *ApJS*, 101, 181
- Yong D., Grundahl F., Lambert D.L., Nissen P.E., Shetrone M.D. 2003, *A&A*, 402, 985
- Zhao G., Magain P. 1990, *A&A*, 238, 242
- Zoccali, M., Barbuy, B., Hill, V., et al. 2004, *A&A*, 423, 507

